การวิเคราะห์รูปแบบและลักษณะการไหลของของไหลเครื่องอบแห้งแบบพ่นฝอย
เพื่อลดการสะสมของอนุภาคที่ผนัง

นางสาวอาทิตยา พัฒนิบูลย์

วิทยานิพนธ์นี้เป็นส่วนหนึ่งของการศึกษาตามหลักสูตรปริญญาวิศวกรรมศาสตรมหาบัณฑิต
สาขาวิศวกรรมเคมี ภาควิชาวิศวกรรมเคมี
คณะวิศวกรรมศาสตร์ จุฬาลงกรณ์มหาวิทยาลัย
ปีการศึกษา ๒๕๕๖
ลิขสิทธิ์ของจุฬาลงกรณ์มหาวิทยาลัย

ANALYSIS OF FUILD FLOW PATTERN AND CONFIGURATION
IN A SPRAY DRYER TO MINIMIZING WALL DEPOSITION PROBLEM

Miss Artitaya Patniboon

Thesis Title   ANALYSIS OF FLUID FLOW PATTERN AND CONFIGURATION IN A SPRAY DRYER TO MINIMIZE WALL DEPOSITION PROBLEM

By   Miss Artitaya Patniboon

Field of Study   Chemical Engineering

Thesis Advisor   Assistant Professor Amornchai Arpornwichanop, D.Eng.

Accepted by the Faculty of Engineering, Chulalongkorn University in Partial Fulfillment of the Requirements for the Master's Degree

....Dean of the Faculty of Engineering

(Professor Bundhit Eua-Arporn, Ph.D.)

THESIS COMMITTEE

....Chairman

(Associate Professor Prasert Pavasant, Ph.D.)

....Thesis Advisor

(Assistant Professor Amornchai Arpornwichanop, D.Eng.)

....Examiner

(Assistant Professor Soorathep Kheawhom, Ph.D.)

....External Examiner

(Assistant Professor Woranee Paengjuntuek, D.Eng.)

อาทิตยา พัฒนิบูลย์ : การวิเคราะห์รูปแบบและลักษณะการไหลเครื่องอบแห้งแบบพ่นฝอยเพื่อลดการสะสมของอนุภาคที่ผนัง (ANALYSIS OF FLUID FLOW PATTERN IN A SPRAY DRYER TO MINIMIZING WALL DEPOSITION PROBLEM) อ. ที่ปรึกษาวิทยานิพนธ์หลัก: ผศ. ดร. อมรชัย อาภรณ์วิชานพ, ๖๔ หน้า

กระบวนการอบแห้งแบบพ่นฝอยเป็นกระบวนการซึ่งนำวัตถุดิบที่เป็นของเหลวใส่ในเครื่องอบแห้ง และได้ผลิตภัณฑ์มีลักษณะเป็นผงของแข็ง ใช้ระยะเวลาสั้นในการอบแห้ง นอกจากนี้ ผลิตภัณฑ์ผงที่ได้มีขนาดและปริมาณความชื้นที่สม่ำเสมอ จากข้อดีดังกล่าวกระบวนการการอบแห้งแบบพ่นฝอยจึงถูกนำมาใช้ในภาคอุตสาหกรรมการอบแห้ง ระหว่างการอบแห้งแบบพ่นฝอย เกิดการชนกันของอนุภาคที่เหนียวนำไปสู่การจับตัวกันเป็นก้อน ในการสัมผัสกัน อนุภาคเหนียวจะเป็นประเด็นสำคัญของปัญหาการสะสมกันของอนุภาคที่ผนัง โดยทั่วไป ตำแหน่งของอนุภาคที่สะสมที่ผนังขึ้นกับลักษณะการไหลของของไหลภายในเครื่องอบแห้ง ซึ่งสามารถทำนายได้ด้วยแบบจำลองพลศาสตร์ของไหลของเครื่องอบแห้งแบบพ่นฝอย เทคนิคจำนวนมากที่ใช้ในการตรวจสอบพฤติกรรมการเหนียว จะให้กราฟของความเหนียวในรูปของ ปริมาณความชื้นของอนุภาค และอุณหภูมิที่เหนียว (sticky temperature: T_s) เป็นความสัมพันธ์ทางอ้อมกับอุณหภูมิการเปลี่ยนสถานะคล้ายแก้ว (glass transition temperature, T_g) ของสสาร ความเหนียวของอนุภาคสามารถอธิบายได้ด้วยค่าอุณหภูมิการเปลี่ยนสถานะคล้ายแก้ว ถูกนำมาเป็นตัวแปรอ้างอิงในกระบวนการและอธิบายสมบัติ, คุณภาพ, ความคงตัว และความปลอดภัยของอาหาร การเปลี่ยนแปลงโครงสร้าง การเติม Carriers Agents หรือ Drying Aids จะช่วยลดความเหนียวของอนุภาคและปัญหาการสะสมของอนุภาคที่ผนังในกระบวนการอบแห้งแบบพ่นฝอย มีการศึกษาเครื่องอบแห้งแบบพ่นฝอยจำนวนมากในห้องปฏิบัติการและในระดับ Pilot Scale แต่อย่างไรก็ตามข้อมูลที่ได้จากเทคนิคการวัดดังกล่าวยังไม่สามารถอธิบายปรากฏการณ์ที่เกิดขึ้นจริงภายในเครื่องอบแห้งแบบพ่นฝอยระดับอุตสาหกรรมได้ ในปัจจุบัน แบบจำลองทางคณิตศาสตร์ได้กลายมาเป็นเครื่องมือที่สำคัญสำหรับการออกแบบและสังเคราะห์กระบวนการ การพัฒนาแบบจำลองส่วนใหญ่อยู่บนพื้นฐานของพลศาสตร์ของไหลเชิงคำนวณ (computational fluid dynamics: CFD) ซึ่งเป็นกระบวนการแก้ปัญหาโดยใช้ระเบียบวิธีเชิงตัวเลขขั้นสูง (advanced numerical methods) เพื่อแก้ปัญหาและวิเคราะห์สมการของแบบจำลองที่อธิบายพลศาสตร์ของไหลภายในกระบวนการอบแห้งแบบพ่นฝอย เพื่อมุ่งศึกษาปัญหาการสะสมของอนุภาคที่ผนังภายในเครื่องอบแห้ง

ภาควิชา : วิศวกรรมเคมี .... ลายมือชื่อนิสิต ....

สาขาวิชา: วิศวกรรมเคมี .... ลายมือชื่อ อ.ที่ปรึกษาวิทยานิพนธ์หลัก....................

ปีการศึกษา ๒๕๕๖ ....

547 04683 21: MAJOR CHEMICAL ENGINEERING

KEYWORDS : SPRAY DRYER / FLUID FLOW / MODELING / ANALYSIS / WALL DEPOSITION PROBLEM

ARTITAYA PATNIBOON : ANALYSIS OF FLUID FLOW PATTERN IN A SPRAY DRYER TO MINIMIZING WALL DEPOSITION. ADVISOR : ASST PROF. AMORNCHAI ARPORNWICHANOP, D.ENG, 64 pp.

Spray drying is one of the widely used processes. The obtained final powder product has specific particle size and moisture content not regarding the dryer capacity and product heat sensitivity. Due to these advantages, spray drying is selected technique for many industrial operations. However, difficulties in spray dryer operation occur as some particles with high moisture content (stickiness) have collected in contacts with metal surface of dryer chamber known as wall deposition problem. Particle deposition, a fluid flow pattern dependent, can be predicted based on a fluid dynamic model. Various developed techniques measure sticky behavior; sticky temperature, T_s, and particle moisture content. An indirect approach correlates between T_s and glass transition temperature, T_g. In general, T_g can be taken as a reference parameter to project the spray drying systems and characterize its properties, including its quality, stability and safety in food systems. Additives agent materials have been used resulting as a reduction of the stickiness and wall deposition in spray dryer. Various studies on spray dryer relied on experiments. However, this information sometimes cannot accurately explain the phenomena within an industrial spray dryer. Mathematical modeling becomes an important tool for process design and synthesis. Most developed models were based on a computational fluid dynamics (CFD) approach in which advanced numerical methods and algorithms are used to solve and analyze the process model equations explaining the fluid dynamics within the process in conducive to the study on wall deposition problem within a spray dryer.

Department   :   Chemical Engineering   Student's Signature

Field of Study : Chemical Engineering   Advisor's Signature

Academic Year : 2013

ACKNOWLEDGEMENTS

The author would like to express appreciation with my greatest gratitude to my thesis advisor, Assistant Professor Dr. Amornchai Arpornwichanop, for his encouraging guidance, discussion and helpful suggestions throughout the course of this master degree study.

The author wishes to especially thank chairman, Associate Professor Dr. Prasert Pavasant and the other members of my thesis committee, Assisant Dr. Soorathep Keawhom and Assisant Dr. Woranee Paengjuntuek for their time and useful comments on this thesis. Many thanks to process control laboratory members, friends, and all those who encouraged through work.

Most of all, the author would like to thank my beloved parents and my sibling for the endless love and encouragement they have given over the years. Without their support, my research work would not have accomplished.

CONTENTS

LIST OF TABLES

LIST OF FIGURES

CHAPTER I

INTRODUCTION

1.1   Importance and Reasons

Drying is the process of removing liquid (usually water) from solids. It helps reduce transport weight and increases the storage life of products; a decrease of the water content in the product reduces a water activity, which causes the product degradation (Hayashi et al., 1989; Chiou et al., 2006). In the past, the drying meant spreading a product out in the open air and letting the sun provide heat for water evaporation. At present, many different drying methods have been developed to increase drying speed and improve product quality and uniformity. These include freeze drying, tray drying, vacuum drying, convective drying, spout and fluidized bed drying and spray drying. The selection of particular drying process depends on type and properties of materials to be processed as well as desired product properties.

Spray drying is one of the widely used processes in which a liquid feed is fed to a dryer and a solid powder product is obtained at the outlet. This method can be seen in various production processsess for food, healthcare and pharmaceutical products. Many biological and thermal sensitive materials, such as herbal drugs, enzymes, essential oils, milk and fruit juices and pulps, have been dried by this process (Cánovas et al., 2005; Masters, 1972) due to a short residence time of the product inside the dryer. In addition, a final powder product has specific particle size and moisture content without regarding the capacity of the dryer and heat sensitivity of product. These advantages make the spray drying be the chosen technique for many industrial drying operations.

In the spray dryer, the liquid feed is first atomized by an atomizer and the obtained liquid droplet is then contacted with hot dried air. At this step, liquid water is evaporated out of the droplet; more than 95% of a total moisture is removed. In general, the type and the position of the atomizer have an effect on the evaporation and the particle size of final powder products (Southwell and Langrish, 2001). Regarding the spray drying process, there are two steps in the evaporation (Dobry et

al., 2009). Firstly, the liquid water at the surface of the droplet is evaporated under a constant rate when the temperature of the droplet surface equals to the wet-bulb temperature of hot air. Secondly, moisture in the internal wet core of the droplet is diffused through the droplet surface and evaporated. The final powder product with desired particle size and moisture content is obtained.

However, operation of the spray dryer may cause some difficulties because some particles having high moisture content (stickiness) do contact the metal surface of a dryer chamber, causing a collection of the particles in the dryer (Kieviet, 1997). This is known as a wall deposition problem. This problem causes a product contamination and affects a quality of the final product (Kuriakose and Anandharakrishnan, 2010) and thus, the spray dryer needed to be clean up at the end of the operation. The wall deposition problem is often occurred when drying amorphous particles with sticky properties. These sticky powders are more hygroscopic and less free flowing than none-sticky powders. Examples of the sticky products are fruit and vegetable juice powders, honey powders and amorphous lactose powders.

The stickiness of powder can be explained by a low glass transition temperature (T_g) of components with low molecular weight (Ozmen and Langrish, 2003). The glass transition temperature is defined as a temperature at which an amorphous system changes from the glassy state to the rubbery state. Molecular mobility in the glassy state is extremely slow, according to high viscosity of the matrix. In general, T_g can be taken as a reference parameter to project the spray drying systems and characterize the properties, quality, stability and safety of food systems. Structural alterations, such as stickiness, agglomeration, caking and crystallization, usually occur in amorphous food powders when stored and processed at temperatures above T_g. Since the glass transition temperature increases with molecular weight, an addition of carriers agents (drying aids) has been used in powder production to reduce the stickiness and wall deposition in the spray drying (Bahandari et al. 1993; Dolinsky et al. 2000; Mujumdar et al. 1987; Welti et al. 1983).

Various studies about the spray dryer have relied on experiments in either laboratory or pilot scale levels (Woo, 2009; Kota and Langrish, 2006; Huntington, 2004). Experimental techniques, such as hot wire anemometry and laser doppler anemometry can be employed to measure flow properties of particles in the spray dryer. However, this valuable information sometimes cannot truly explain the phenomena within an industrial spray dryer (Huang et al., 2006). Nowadays, mathematical modeling becomes an important tool for process design and synthesis. Literature survey demonstrates that during the last decades, advanced two- and three-dimensional models of the spray dryer have been proposed by several academic and industrial groups (Fletcher et al., 2003; Fletcher et al., 2006; Huang et al., 2006). Most of the developed models were based on a computational fluid dynamics (CFD) approach in which advanced numerical methods and algorithms are used to solve and analyze the process model equations explaining the fluid dynamics within the process itself. The CFD-based model reveals the complexity of flow fields of drying agent and droplets/particles. Although the internal transport phenomena of spray drying processes has been widely reported (Langrish et al., 2004), there have been few studies that have focused on investigating the wall deposition problem in the spry dryer. The fluid flow pattern of droplet particles within the spray dryer affects final product quality and wall deposition of droplet particles as well; however, this behavior is difficult to be measured from experiment. A computational modeling of the spray dryer is applied to predict the droplet flow pattern, leading to an understanding of the wall deposition problem.

1.2 Objective

The objective of this research is focused on the analysis of a fluid flow pattern and key operating parameters within a spray dryer using a fluid dynamics model.

1.3 Scopes

1. The fluid dynamic model of a co-current spray dryer is developed and solved by a finite element method.

2. The drying process of an anthocyanin solution (density = 1,240 kg/m^3, dynamic viscosity = 3.588×10^{-4} mPa·s and concentration = 50 wt.%) is chosen as a case study.

3. Simulations of the spray dryer under the steady state condition are performed to investigate the flow pattern of droplet particles and to predict the position of droplet wall deposition within the spry dryer.

4. Key operating parameters to be studied are feed rate, heat transfer coefficient, drying agent material and configuration of spray dryer.

1.4   Contribution

To understand the effect of a fluid flow pattern and key operating parameters on the wall deposition problem of droplet particles in the spray dryer.

1.5   Dissertation Overview

Chapter II reviews the past works related to spray drying, concept of spray drying and wall deposition problem.

Chapter III mentions the details of the theory of spray dry including basic of spray drying method and theory of spray drying process.

Chapter IV mentions mathematical model of spray dryer are used in computational fluid dynamic solver and validation model including comparison between measurements and predictions result.

Chapter V explains the prediction of wall deposition problem on fluid flow pattern and key parameter. In addition to, simulated results of the viscous stress, glass transition temperature, sticky-point temperature and wall heat transfer coefficient are examined and discussed.

Chapter VI gives the summary and suggestions of this dissertation.

CHAPTER II

LITERATURE REVIEWS

The concept of spray drying is based on the high increase in the surface area of the contact area between the material to be dried and the drying medium promoted by the atomization. The variables generally monitored during spray drying include the inlet and outlet drying gas temperature and humidity and the feed flow rate of drying gas and liquid material. These data can be used to predict and to improve the efficiency of the drying process, through performing mass and energy balances, statistical analysis and/or process simulations (Oliveira et al., 2010).

During spray drying, water evaporates from the surface and the viscosity of the droplet surface increases and reaches to a critical value (10^7 Pa·s) (Roos and Karel, 1991) which the particle surface is in a rubbery state that is considered as sticky. Surface stickiness depends on surface temperature, water content and composition (i.e. carbohydrates and fats). When the surface reaches to the rubbery state, collisions with other particles (sticky or dry) could lead to agglomeration, depending on velocity, force, angle and time of contact between particles (Huntington, 2004; Palzer, 2005). Particle stickiness is a key issue in wall deposition for spray dryers. In general, the position of particle deposition on the wall depends on the fluid flow pattern in the dryer and can be predicted based on a fluid dynamic model of the spry dryer (Masters, 1996).

The experimental and numerical investigations of air flow in co-current pilot plant spray dryer at no swirl proved that air flow can be characterized by the central air core bounded by slow recirculation zones (Oakley et al. 1988; Le Barbier et al. 2001). Bigger particle sizes penetrated the core and stilled in the recirculation zones for more time which lead to hitting the wall or depositing if it in the sticky case (Kieviet, 1997). For example, Chegini and Ghobadian (2004) studied the effect of drying parameters on the laboratory spray dryer for the fruit juice powder production. They investigated the stickiness of powder and the natural characteristics of fruit juice, which causes no powder production. The statistical analysis of experimental data showed that the inlet air temperature and the feed flow rate are among the key parameters affecting the dryer yield and the wall deposit of spray dryer (Chegini and Ghobadian, 2004).

Various techniques have been developed to measure the sticky behavior (Boonyai et al., 2004). All these techniques provide a stickiness curve in term of the sticky temperature, T_s, and the particle moisture content. An indirect approach correlates the sticky temperature, T_s, to the glass transition temperature, T_g, of the substance; in general, T_s is 10 to 30 degrees higher than T_g (Roos and Karel, 1991).

This correlation was used to the development of adhesiveness and cohesiveness of single droplet during drying (Werner, 2007).

Ozmen and Langrish (2003) investigated the wall deposition effect in a pilot scale spray dryer unit and developed the deposition model based on the Glass Transition – Sticky Point concept. Figure 2.1 show that the glass transition temperature (and the corresponding sticky point temperature) is a strong function of the particle moisture. At higher moisture contents, the sticky point becomes lower and vice versa. If the particle temperature is above the sticky point, the particle is then deemed sticky and will adhere to the walls of the processing equipment (Ozmen and Langrish, 2003).
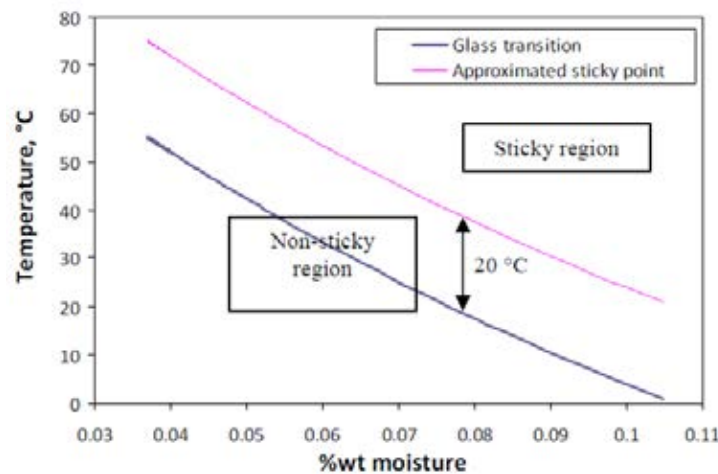
Figure 2.1 Typical glass transition and approximated sticky point curve for lactose. (Ozmen and Langrish, 2003)

However, it is noteworthy that the concept of using the glass transition as the cut-off point does not account for the effect of impacting velocity and angle on the collision outcome.

2.1 Modeling of spray dryer

In general, changes in the flows of air and particle and the droplet surface properties during spray drying processing are difficult to explain. In recent years, computational fluid dynamics (CFD) has been increasingly applied to modeling food processing operations (Kuriakose and Anandharakrishnan, 2010). A number of theoretical, numerical studies on the analysis of air flow patterns in the spray dryer have been published. The CFD of air flow pattern has proven to be a very useful tool to predict the flow behavior in complex geometries of spray dryers (Fletcher et al., 2006).

Langrish (2009) has reviewed the detailed form of the governing equations to describe the spray dryer. In modeling of the dryer, the assumption of uniformity rarely occurs in practice and more rigorous models describing gradual changes in the field properties are required. The result is known as the finest-scale modeling, which uses the CFD as a tool for simulating the transport phenomena within the dryer.

Most spray dryer CFD simulations reported were performed by using commercial softwares, such as FLUENT, CFX, STAT3D (Woo et al., 2009; Ullum, 2006; Langrish et al., 2004; Verdumen et al., 2004; Kajiyama and Park, 2010). The turbulence model was used because the chamber Reynolds number is higher than 2000, which is usually in the turbulent regime. In addition, all the CFD simulations used the Reynolds Averaged Navier-Stokes (RANS) approach in which the large scale turbulent eddies are modeled. Straatsma et al. (1999) and Langrish and Zbicinski (1994) used the CFD simulations to assess the effect of cone spray angle on the deposition problem.

The CFD model can also be used for process optimization. Lo (2005) used the CFD model to determine the optimal operating conditions of the spray tower in term of air flow rate to achieve the desired quality of the dairy products. Optimization was performed by considering the yield, moisture and temperature of particles at the outlet.

2.2 Particle stickiness problem

Two ways for preventing of stickiness were, using of drying agent material and using of specific equipment to facilitate the powder handling (Chegini, G.R. and B. Ghobadian, 2004).

2.2.1 Drying agent material

Particles hygroscopic reduction required drying agent materials. Additives agent materials have been used to produce physical changes in the product, consequently reducing the stickiness and wall deposition in spray drying. These agent materials include corn syrup; natural gums, sucrose, maltodextrin etc…caused powder production and prevent cohesion of particle on spray dryer wall (Bahandari et al. 1993; Dolinsky et al. 2000; Mujumdar et al. 1987; Welti et al. 1983). Chegini and Ghobadian added liquid glucose, the optimum conditions have been obtained with feed flow rate of 15 ml min 1, inlet air temperature of 130°C and outlet air temperature of 85°C. For the orange powder containing 2% moisture, the sticky point temperature was 44°C (Chegini, G.R. and B. Ghobadian, 2004).

2.2.2 Specific equipment to facilitate the powder handling

A recent review suggested that the properties of the wall material, specifically its surface energy, do affect wall deposition and future analysis should be considered both the droplets and wall surface of system (Bhandari et al., 2005). Bhandari and coworkers had shown that Teflon is generally less sticky when compared to stainless steel by using an in situ tack method for relatively large droplets, (Adhikari et al., 2007) the applicability of the data to the actual spray-drying process has not been proven experimentally. Langrish, using similar methods, had shown the effect of the wall materials is not significant, (Ozmen and Langrish, 2003) but a later work by Kota and Langrish (2006) showed that nylon exhibited lesser deposition when compared to stainless steel.

Particles build up due to the adhesion of particles to initially clean walls of spray dryers. Subsequent layers of particles become attached to this initial layer (cohesion). Woo (2012) observe the effect of wall material on the adhesion flux at different particle surface wetness and rigidity in an actual pilot-scale spray dryer. Surface energy and surface roughness were found to have no significant effect for dry rigid particles at the middle and bottom elevation of the drying chamber. However, material with lower surface energy (Teflon) exhibited less deposition for rubbery particles at such elevations. As expected, material with lower surface energy (Teflon) exhibited lesser deposition for rubbery particles at the middle and bottom elevations. The effect of wall temperature on the deposition of rubbery particles was confirmed in a pilot-scale spray dryer. Teflon exhibited another disadvantage in the deposition of dry particles since the accumulation of charges (due to abrasion on dielectric material) on the surface causes more particles to adhere. This is one disadvantage of using dielectric wall material (normally lower surface energy) to solve the deposition problem (Woo, 2012).

Other methods try to control the surrounding product or air temperatures, such as using appropriate outlet drying air temperature (Bhandari et al., 1997b) or introducing cold air into the bottom part of the dryer (Lazar et al., 1956) or cooling the wall temperature (Brennan et al., 1971). The improvement of spray drying performance while applying these methods to reduce stickiness has been reviewed (Bhandari et al., 1997a).

The literature shows many possibility mechanisms of particle stickiness and wall deposition problem, method of prevented stickiness were using of drying agent material and using of specific equipment to facilitate the powder handling. In addition, it shows several other examples of the spray drying to reduce wall deposition problem. The objective of this study is to predict the possible position of wall deposition problem by shear stress and glass transition temperature at the wall

and to minimize operating condition of feed and air rate and configuration of spray dryer for reducing wall deposition problem.

CHAPTER III

THEORY OF SPRAY DRYING

3.1 A basic of spray drying method

Spray drying is widely used in powder product such as milk, coffee, drug and washing powder etc. Its high performance drying, high heat exchanging rate, short drying time and less contamination because of it is a closed system. That is provided avoidance from chemical substances or biological degradation, further storage volume reduction has lessen the cost of transportation including continuous operating system maintenance.
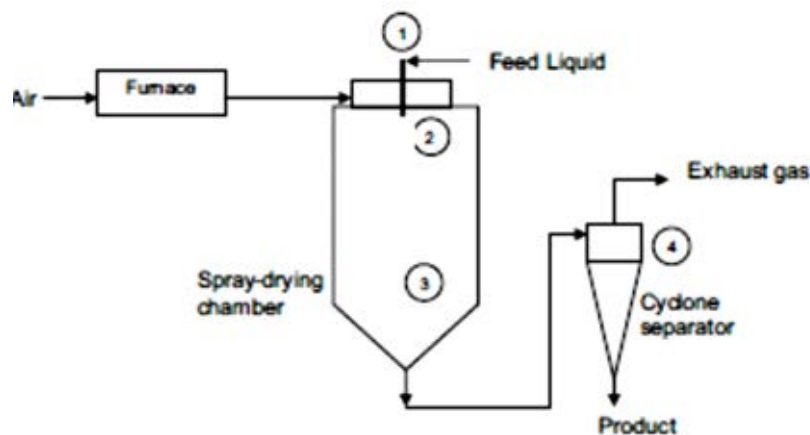
Figure 3.1 Spray drying technique. (Kuriakose and Anandharamakrishnan, 2010)

3.1.1 Principle of spray drying system

Spray drying technique is a method of evaporating water out of liquid solution rapidly by injected hot dried air. This process consists of feed atomization, introduced feed in a droplet form which a contact with the hot dried air results in water in the droplet evaporation and dried powder product is obtained. Schematic of spray drying process started with feeding solution into the dryer until suitable moisture content solution is appropriate for atomization. Then through drying process, dried powder is separated at the bottom of the dryer. Liquid feed of drying process can be use in emulsion solvent or suspension forms. In addition, the only equipment used in this process is spray dryer.

3.1.2 Theory of spray drying process

Spray drying process can be classified into four steps, as follows;

1) Atomization: Atomization is the main principle of spray drying process Because of its increasing evaporation surface area, rapidly evaporated water and specified droplet in its physical characteristics, configurations and density. The size of liquid droplet is reduced, thus increased heat exchanging area has caused heat and mass to efficiently exchanged.

2) Atomization of Feed: this process atomizes liquid feed into the droplets by atomizer which is the most important component in spray dryer. Several type of atomization can be employed in a spray drying system. The droplet size from a given type of atomization device depends on the energy spent for breaking down the liquid into fragments that is, increasing the overall surface of the liquid. For most atomization systems, the liquid does not leave atomizing head as a droplet, but as a fragment of a thin liquid film. The droplet formation takes place immediately after liquid has left the atomizing head during the surface tension of a perfect droplet is therefore very dependent on the rheological properties of the liquid and the interaction with hot dried air just outside atomizing device. There are 3 types of Atomizers (Thousig Moller and Fredsted, 2009).

Figure 3.2 Rotary Atomizer.

2.1 Rotary or Centrifugal Atomizer: Rotary atomization is the most common form of atomization. This equipment's liquid feed flows down from a rotary dish near the center with angular velocity around 5,000-25,000 rpm. Discs or wheels typically have a diameter of 5-50 cm. The size of droplets produced is nearly inversely proportional to the peripheral speed of the wheel. Fallen liquid feed on the rotary dish is then centrifuged to a side, dispersed its configuration droplets ranged 30-120 μm.
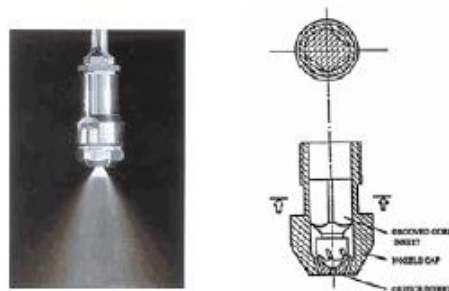
Figure 3.3 Pressure Nozzles Atomizer.

2.2 Pressure Nozzles Atomizer: liquid feed flows through the orifice of a nozzle at high pressure caused dispersion of liquid without air. This limits the capacity of a nozzle to approximately 750-1,000 kg/h of liquid feed, depending also on pressure, viscosity and the solids content of the liquid feed. The configuration droplet is at 120-150 μm which is proportional with size of the orifice and the pressure drop. A larger pressure drop across the orifice produces smaller droplets. Therefore, to reduce the particle size for a given feed flow rate, a smaller orifice and a higher pump pressure must be provided to achieve the same mass flow through the nozzle.
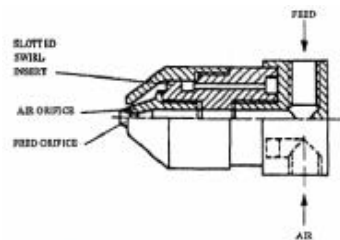
Figure 3.4 Two-fluid Nozzle Atomizer.

2.3 Two-fluid Nozzle Atomizer or Pneumatic Nozzle Atomizer: Two-fluid nozzle atomization is primarily used in smaller drying systems. Atomization is accomplished by the interaction of feed with a second fluid usually compressed air. Sprayed liquid feed and air streams through a nozzle which liquid feed is broken into droplets caused by high velocity of air in a nozzle. Air volumetric flow rate helps disperse droplets. This preferred type is aim to use with high viscous liquid although its operating cost is insufficient with its low output.

3) Droplet - air contact: Focusing on the single droplet, it is contacted with the hot dried air for water/moisture evaporation in order for the heat from hot dried air transferred to liquid feed. Determination of hot dried air direction is important to consider whether it is suitable direction, its rapid heat transfer depends on purpose, required quality and characteristic of product. This contact has been categorized 3 types.
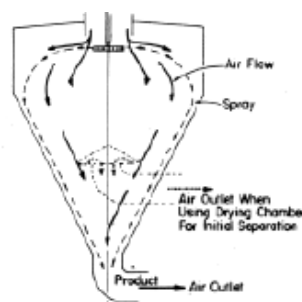
Figure 3.5 Co-current flow.

3.1 Co-current flow: sprayed liquid feed is directed into the hot dried air entering the dryer which both passed though chamber in the same direction. This type is a preferred design for heat sensitive products because of the hottest drying air contacts at droplets' maximum moisture content. Spray evaporation is rapid, and the temperature of dried air is quickly reduced by water vaporization. The product does not suffer from heat degradation because the droplet temperature is low enough during most of the evaporation time.
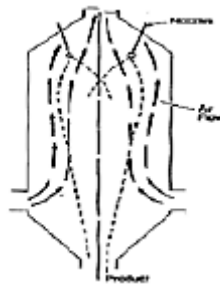
Figure 3.6 Counter-current flow.

3.2 Counter-current flow: sprayed liquid feed and air are introduced at opposite ends of the dryer, with an atomizer positioned at the top and air entering at the bottom. Starting from low temperature feed, its temperature increased steadily as heat being transferred from hot air in contact until its temperature reached the same point. A counter-current dryer offers more rapid evaporation and higher energy efficiency than a co-current dryer design. Because dried product is in contact with hottest air, this design is not suitable for heat sensitive products.
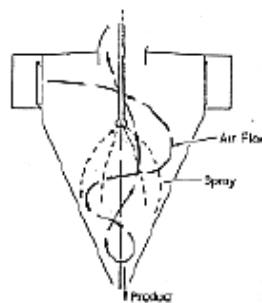
Figure 3.7 Mixed-flow

3.3 Mixed-flow: this design combines both co-current and counter-current flow. In a mixed-flow dryer, air entered at the top and atomizer located at the bottom. Like counter-current design, mixed flow exposure dried product to hot dried air, so this design is not suitable for heat sensitive products.

4) Droplet evaporation: A saturated stream at the droplet surface is rapidly evaporated when droplet contacts with hot dried air. Wet bulb temperature at droplet surface in a saturated condition is diffused to surface with a constant evaporation rate until it has low moisture which it's not diffused cause of dried layer depend on the time.

3.2 Critical parameters of spray drying

1) **Inlet temperature of air:** higher the temperature of inlet air, faster is the moisture evaporation but the powder is subjected to higher temperature, which may distort the chemical/physical properties of heat sensitive product.

2) **Outlet temperature of air:** it govern the sizing of powder recovery equipments, higher is the outlet air temperature larger will be the size of powder recovery equipment and conveying ducts and plenums. Outlet air temperatures control final moisture content of powder.

3) **Viscosity:** high viscosity hinders correct drop formation. As the viscosity is lowered, less energy or pressure is required to form a particular spray pattern.

4) **Solid content:** care must be taken with high solid loadings (above 30%) to maintain proper atomization to ensure correct droplet formation.

5) **Surface tension:** addition of a small amount of surfactant can significantly lower the surface tension. This can result in a wider spray pattern, smaller droplet size, and higher drop velocity.

6) **Feed temperature:** as the temperature of a solution to be sprayed is increased, the solution may easily dry as it brings more energy to the system.

7) **Volatility of solvent:** a high volatility is desirable in any drying process. Unfortunately, choices are limited today. In many cases, these restrict the solvent choice to water.

8) **Nozzle material:** most pharmaceutical applications use stainless steel inserts. However, tungsten carbide nozzles are often available and have excellent resistance to abrasion and good corrosion resistance for most feedstock.

CHAPTER IV

COMPUTATIONAL FLUID DYNAMICS (CFD)

4.1 Mathematical model of spray dryers

This section gives a brief overview of the CFD solver used in this study which is the FLUENT software from FLUENT Inc.. For further detailed information, which is not covered in the following sections, the interested reader is referred to the software User's Guide [FLUENT, 2004].

The FLUENT 6.1 CFD package consists basically of two components: (1) GAMBIT 2.0, the pre-processor and (2) FLUENT 6.1, the solver. The pre-processor "GAMBIT" was used to create the model of the actual fluid-laden geometry in two dimensions (2D) or three dimensions (3D). Using this pre-processor, the geometry was subdivided in a grid (or mesh) consisting of cells which form the calculation domain for the subsequent flow analysis. The grids can either be structured where each cell is part of a rectangular block structure and follow the Cartesian co-ordinate system or it could be totally unstructured. The cells may be of quadrilateral or triangular shape for 2D-meshes. Three dimensional meshes may consist of hexahedral, tetrahedral, wedge-shape elements or pyramids or combinations of them.

Furthermore, GAMBIT allows examining the quality of the mesh by assessing the various aspects of cell quality (e.g. the aspect ratio of a quadrilateral cell). In general, to obtain a mesh-independent solution, the mesh resolution needs to be fine. For the 2D-calculations, the mesh was therefore refined until the solution became mesh-independent. This could also be done to a certain extent with 3D-meshes. The meshes also can be refined locally by *grid adaptation*, where necessary. After completing the pre-processing, the mesh is then exported to the solver FLUENT 6.1.

The solver FLUENT 6.1 is used to select the appropriate physical models specifying the current problem. For example, (1) the flow regime: laminar/turbulent conditions; (2) the problem type: steady state/transient conditions; (3) the fluid properties: incompressible/compressible; (4) the detailed problem specification such as boundary conditions, materials and injectors.

In addition to this, a solver formulation and solution parameters have to be chosen. Finally, an initial solution for all cells must be provided. The underlying governing equations will then be solved in an iterative process for each individual cell of the calculation domain.

The post-processing, i.e. the graphical illustration of the results, can be done by FLUENT 6.1.

In this study, all geometry and meshing works were carried out with GAMBIT 2.0. All calculation works have been carried out with FLUENT 6.1 on UNIX platform.

4.1.1 Governing equations for the continuous phase

For any fluid, its flow must obey the conservation of mass and momentum. These conservation equations can be found in standard fluid dynamic literature (for incompressible gas) [Bird, Stewart and Lightfoot, 1960; Ferziger & Peric, 1999]

The general form of the continuity equation for mass conservation is

$$\frac{\partial \rho}{\partial t} + \frac{\partial (\rho u_i)}{\partial x_i} = M_m \tag{4.1}$$

The general form of the equation for momentum conservation is

$$\frac{\partial (\rho u_i)}{\partial t} + \frac{\partial (\rho u_i u_j)}{\partial x_i} = -\frac{\partial P}{\partial x_j} + \frac{\partial}{\partial x_i}\left[\mu(\frac{\partial u_i}{\partial x_j} + \frac{\partial u_j}{\partial x_i}) - \rho\overline{u_i'u_j'} \right] + \rho g_i + M_F \tag{4.2}$$

This is in accordance with Newton's law (mass times acceleration = sum of forces) where the first term on the left-hand side of equation (3.2) is dedicated to the rate of increase of momentum per unit volume and the second term is the momentum increase/decrease per unit volume due to convection. The first term on the right-hand side of equation (3.2) is the pressure force on a fluid element per unit volume, the second term is the viscous force on a fluid element per unit volume and the third term is the gravitational force on a fluid element per unit volume. The last term is M_F the momentum source term.

For Newtonian fluids, the components of the stress tensor can be written as τ_{ij} in equation (3.2)

$$\tau_{ij} = \mu(\frac{\partial u_i}{\partial x_j} + \frac{\partial u_j}{\partial x_i}) - \frac{2}{3}\delta_{ij}\frac{\partial u_i}{\partial x_i}$$

with the fluid viscosity μ and the volume dilation term with the 'Kronecker' delta:

$$\delta_{ij} = \begin{cases} 1\, for = j \\ 0\, for \neq j \end{cases}$$

The general form of the energy equation is

$$\frac{\partial(\rho c_p \mathrm{T})}{\partial t} + \frac{\partial(\rho c_p u_i \mathrm{T})}{\partial x_i} = \frac{\partial}{\partial x_i}\left[k\frac{\partial T}{\partial x_i} - \overline{\rho u_i' T'}\right] + M_h \tag{4.3}$$

Most spray dryers have flow that is axi-symmetric. So, if the cylindrical ordinate system is used, the above equations for air at steady operations can be expressed as

* Continuity equation

$$\frac{\partial}{\partial t}(\mathrm{u}\,\rho_g) + \frac{1}{r}\frac{\partial}{\partial r}(\mathrm{r}\,v\rho_s) = S_i \tag{4.4}$$

* Momentum equation

Axial momentum:

$$\frac{\partial}{\partial t}(\rho_g \mathrm{u}^2) + \frac{1}{r}\frac{\partial}{\partial r}(\mathrm{r}\,\rho_s uv) = \frac{\partial}{\partial x}\left[\left(\mu_L + \mu_T\right)\frac{\partial u}{\partial x}\right] + \frac{1}{r}\frac{\partial}{\partial r}\left[\left(\mu_L + \mu_T\right)r\frac{\partial u}{\partial r}\right] - \frac{\partial P}{\partial x} +$$
$$\frac{\partial}{\partial x}\left[\left(\mu_L + \mu_T\right)\frac{\partial u}{\partial r}\right] + \frac{1}{r}\frac{\partial}{\partial r}\left[\left(\mu_L + \mu_T\right)r\frac{\partial v}{\partial x}\right] + M_u \tag{4.5a}$$

Radial momentum:

$$\frac{\partial}{\partial x}(\rho_g \mathrm{u}\,v) + \frac{1}{r}\frac{\partial}{\partial r}(\mathrm{r}\,\rho_g uv^2) = \frac{\partial}{\partial x}\left[\left(\mu_L + \mu_T\right)\frac{\partial v}{\partial x}\right] + \frac{1}{r}\frac{\partial}{\partial r}\left[\left(\mu_L + \mu_T\right)r\frac{\partial v}{\partial r}\right] -$$
$$\frac{\partial P}{\partial r} + \frac{\partial}{\partial x}\left[\left(\mu_L + \mu_T\right)\frac{\partial u}{\partial r}\right] + \frac{1}{r}\frac{\partial}{\partial r}\left[\left(\mu_L + \mu_T\right)r\frac{\partial v}{\partial x}\right] + \frac{\rho_g w^2}{r} + M_v \tag{4.5b}$$

Tangential momentum:

$$\frac{\partial}{\partial x}(\rho_g \mathrm{urw}) + \frac{1}{r}\frac{\partial}{\partial r}(\mathrm{r}\,\rho_g vrw) = \frac{\partial}{\partial x}\left[\left(\mu_L + \mu_T\right)\frac{\partial(\mathrm{rw})}{\partial x}\right] + \frac{1}{r}\frac{\partial}{\partial r}\left[\left(\mu_L + \mu_T\right)r\frac{\partial(\mathrm{rw})}{\partial r}\right]$$
$$-\frac{2}{r}\frac{\partial}{\partial r}\left[r\left(\mu_L + \mu_T\right)w\right] + M_w \tag{4.5c}$$

The energy conservation equation for gas can be written as

$$\frac{\partial}{\partial x}(\rho_g \mathrm{uq}) + \frac{1}{r}\frac{\partial}{\partial r}(\mathrm{r}\,\rho_g vq) = \frac{\partial}{\partial x}\left[\left(\mu_L + \frac{\mu_T}{\sigma_h}\right)\frac{\partial q}{\partial x}\right] + \frac{1}{r}\frac{\partial}{\partial r}\left[\left(\mu_L + \frac{\mu_T}{\sigma_h}\right)r\frac{\partial q}{\partial r}\right] + M_h \tag{4.6}$$

where, u,v,w are the average axial velocity, radial velocity and tangential velocity of gas, respectively; q is the enthalpy of gas; M_h is the rate of heat transfer between the

droplets and the gas. Also, M_w, M_v, M_u are the rate of momentum between droplets and gas in the axial, radial and tangential directions, respectively. q the laminar viscosity of the fluid is μ_L and the turbulent viscosity is described by μ_T.

4.1.2 Governing equations for the particle

Based on the solution obtained for the flow field of the continuous phase, using an Euler-Lagrangian approach we can obtain the particle trajectories by solving the force balance for the particles taking into account the discrete phase inertia, aerodynamic drag, gravity g_i and further optional user-defined forces F_{xi}.

$$\frac{\partial u_{pi}}{\partial x} = C_D \frac{18\mu}{\rho_p d_p^2} \frac{Re}{24} (\mu_i + \mu_{pi}) + g_i \frac{\rho_g - \rho}{\rho_g} + F_{xi} \tag{4.7}$$

with particle velocity μ_{pi} and fluid velocity μ_i in direction, particle density ρ_p , gas density ρ_g , particle diameter d_p and relative Reynolds number

$$Re = \frac{\rho d_p |u_p - u|}{\mu} \tag{4.7a}$$

and drag coefficient

$$C_D = a_1 + \frac{a_2}{Re} + \frac{a_3}{Re^2} \tag{4.7b}$$

where a_1, a_2 and a_3 are constants [Fluent, 2004].

Two-way coupling allows for interaction between both phases by including the effects of the particulate phase on the fluid phase. Further, the particles are assumed to be fully dispersed, i.e. they are not interacting with each other.

The particle trajectory is updated in fixed intervals (so-called length scales) along the particle path. Additionally, the particle trajectory is updated each time the particle enters a neighboring cell. FLUENT in general interpolates the gas velocity to the particle position assuming linear interpolation.

4. 1.3 Turbulence models

4. 1.3.1 Governing equations for different turbulence Models

In turbulent flows, the instantaneous velocity component μ_i is the sum of a time-averaged (mean) $\overline{\mu_i}$ value and a fluctuating component μ_i , as shown in equation (4.9).

$$u_i = \bar{u}_i + u_i'$$

$$(4.9)$$

These fluctuations need to be accounted for in the above illustrated NAVIE-STOKES equation (4.10)

$$\frac{\partial}{\partial t}(\rho u_i) + \frac{\partial}{\partial x_j}(\rho u_i u_j) = -\frac{\partial P}{\partial x_i} + \frac{\partial}{\partial x_j}\left[\mu\left(\frac{\partial u_i}{\partial u_j} + \frac{\partial u_j}{\partial x_i} - \frac{2}{3}\delta_{ij}\frac{\partial u_i}{\partial x_i}\right)\right] + \frac{\partial}{\partial x_j}\left(-\rho\overline{u_i'u_j'}\right)$$

$$(4.10)$$

Compared with equation (4.2), equation (4.10) contains an additional term $-\rho\overline{u_i u_j}$, the so-called *Reynolds stress* which represents the effect of turbulence and must be modeled by the CFD code. Limited computational resources restrict the direct simulation of these fluctuations, at least for the moment. Therefore, the transport equations are commonly modified to account for the averaged fluctuating velocity components. Two commonly applied turbulence modeling approaches have been used in the present studies: k-ε model [Launder et al., 1972 and 1974]/a RNG k-ε model [Yakhot and Orszag, 1986; Choudhury, 1993] and a Reynolds stress model (RSM)[Launder, Reece and Rodi, 1975; Gibson and Launder, 1978; Launder, 1989].

The standard k-ε model focuses on mechanisms that affect the turbulent kinetic energy. Robustness, economy, and reasonable accuracy over a wide range of turbulent flows explain its popularity in industrial flow and heat transfer simulations. Two variants of this model are available in FLUENT: the RNG k-ε model and the realizable k-ε model [Shih, Liou, Shabbir and Zhu, 1995]. The RNG k-ε model was derived using a rigorous statistical technique (called Re-Normalisation Group theory). It is similar in form to the standard k-ε model, but the effect of swirl on turbulence is included in the RNG mode enhancing accuracy for swirling flows. The realizable k-ε model contains a new formulation for the turbulent viscosity, and a new transport equation for the dissipation rate is derived from an exact equation for the transport of the mean-square vorticity fluctuation [FLUENT, 2004].

The standard k-ε model and its variants (k-ε RNG model etc.) have become popular turbulence models for calculating typical engineering problems with CFD. These models apply the so-called Boussinesq hypothesis [Hinze, 1975] to describe the Reynolds stresses as a function of the velocity gradients and the turbulent viscosity μ_t as follows:

$$\rho\overline{u_i'u_j'} = \mu\left(\frac{\partial u_i}{\partial x_j} + \frac{\partial u_j}{\partial x_i}\right) - \frac{2}{3}\left(\rho k + \mu_t\frac{\partial u_i}{\partial x_i}\right)\delta_{ij}$$

$$(4.11)$$

Two additional transport equations have to be solved, one equation for the turbulent kinetic energy k, and another for the turbulence dissipation rate ε. The turbulent viscosity μ_t is computed as

$$\mu_t = \rho c_\mu \frac{k^2}{\varepsilon} \tag{4.12}$$

with the empirical constant $c_\mu = 0.009$ [Launder and Spalding, 1972]. The advantages of the k-ε model are its robustness and the fact that only two additional transport equations need to be solved. On the other hand, the turbulent viscosity is assumed to be an isotropic quantity which can be a questionable simplification especially when modeling the swirling flows or flows with regions with high and low Reynolds number. The k-ε RNG model can be used to treat turbulent flows with swirl. For high-Reynolds number the equation (4.12) is still suitable with a c_μ value of 0.0845.

The RSM solves transport equations for all Reynolds stresses and the dissipation rate ε and therefore does not rely on the isotropic turbulent viscosity μ_t. This makes the RSM suitable to predict even swirling flows, however, the major drawback of this model is computational effort needed to solve these equations. For 3D-simulations, seven additional transport equations must be solved (six for the Reynolds stresses and one for the dissipation rate ε). However, the RSM is highly recommended if the expected flow field is characterized by anisotropy in the Reynolds stresses as is the case with swirling flows e.g. cyclones or spray drying with tangential inlet ducts. Crowe [1980] emphasized that the k-ε model is not suitable for swirl flow problems.

The transport equations for the standard k-ε model are for transport of the turbulence kinetic energy, k, and its dissipation rate, ε. They are:

$$\frac{\partial(\rho k)}{\partial t} + \frac{\partial(\rho k u_i)}{\partial x_i} = \frac{\partial}{\partial x_j}\left[\left(\mu + \frac{\mu_t}{\sigma_k}\right)\frac{\partial k}{\partial x_j}\right] + G_k + G_b - \rho\varepsilon - Y_M + S_k \tag{4.13}$$

and

$$\frac{\partial(\rho\varepsilon)}{\partial t} + \frac{\partial(\rho\varepsilon u_i)}{\partial x_i} = \frac{\partial}{\partial x_j}\left[\left(\mu + \frac{\mu_t}{\sigma_\varepsilon}\right)\frac{\partial\varepsilon}{\partial x_j}\right] + C_{1\varepsilon}\frac{\varepsilon}{k}(G_k + C_{3\varepsilon}G_b) - C_{2\varepsilon}\rho\frac{\varepsilon^2}{k} + S_\varepsilon \tag{4.14}$$

The turbulence viscosity, μ_t, is computed using equation (4.12)

The model constants values, i.e., $c_{1\varepsilon}, c_{2\varepsilon}, c_\mu, \rho_k$ and ρ_ε, are set to the following values [Launder and Spalding, 1972]:

$$C_{1\varepsilon} = 1.44, C_{2\varepsilon} = 1.92, C_{\mu} = 0.09, \sigma_k = 1.0, \sigma_{\varepsilon} = 1.3$$

The turbulence kinetic energy, k, and its dissipation rate, ε, for RNG k-ε turbulence model are

$$\frac{\partial(\rho k)}{\partial t} + \frac{\partial(\rho k u_i)}{\partial x_i} = \frac{\partial}{\partial x_j}\left[\alpha_k \mu_{eff} \frac{\partial k}{\partial x_j}\right] + G_k + G_b - \rho\varepsilon - Y_M + S_k \qquad (4.15)$$

and

$$\frac{\partial(\rho\varepsilon)}{\partial t} + \frac{\partial(\rho\varepsilon u_i)}{\partial x_i} = \frac{\partial}{\partial x_j}\left[\alpha_k \mu_{eff} \frac{\partial\varepsilon}{\partial x_j}\right] + C_{1\varepsilon}\frac{\varepsilon}{k}(G_k + G_{3b}) - C_{2\varepsilon}\rho\frac{\varepsilon^2}{k} + S_{\varepsilon} \qquad (4.16)$$

The turbulence kinetic energy, k, and its dissipation rate, ε, for Realizable k-ε turbulence model are

$$\frac{\partial(\rho k)}{\partial t} + \frac{\partial(\rho k u_i)}{\partial x_i} = \frac{\partial}{\partial x_j}\left[\left(\mu + \frac{\mu_t}{\sigma_k}\right)\frac{\partial k}{\partial x_j}\right] + G_k + G_b - \rho\varepsilon - Y_M + S_k \qquad (4.17)$$

and

$$\frac{\partial(\rho\varepsilon)}{\partial t} + \frac{\partial(\rho\varepsilon u_i)}{\partial x_i} = \frac{\partial}{\partial x_j}\left[\left(\mu + \frac{\mu_t}{\sigma_{\varepsilon}}\right)\frac{\partial\varepsilon}{\partial x_j}\right] + \rho C_1 S_{\varepsilon} - \rho C_2 \frac{\varepsilon^2}{k + \sqrt{v\varepsilon}} + C_{1\varepsilon}\frac{\varepsilon}{k}C_{3\varepsilon}G_b + S_{\varepsilon}$$
$$(4.18)$$

The governing equations for the RSM model are as follows [FLUENT, 2002]

$$\frac{\partial}{\partial t}\left(\rho\overline{u_i'u_j'}\right) + \frac{\partial}{\partial x_k}\left(\rho u_k\overline{u_i'u_j'}\right) = -\frac{\partial}{\partial x_k}\left[\rho\overline{u_i'u_j'u_k'} + \overline{p\left(\delta_{kj}u_i' + \delta_{ik}u_j'\right)}\right] + \frac{\partial}{\partial x_k}\left[\mu\frac{\partial}{\partial x_k}\left(\overline{u_i'u_j'}\right)\right]$$

$$-\rho\left(\overline{u_i'u_k'}\frac{\partial u_j}{\partial x_k} + \overline{u_j'u_k'}\frac{\partial u_i}{\partial x_k}\right) - \rho\beta\left(g_i\overline{u_j'\theta} + g_j\overline{u_i'\theta}\right) + \overline{p\left(\frac{\partial u_i'}{\partial x_j} + \frac{\partial u_j'}{\partial x_i}\right)} - 2\mu\overline{\frac{\partial u_i'}{\partial x_k}\frac{\partial u_j'}{\partial x_k}}$$

$$-2\rho\Omega_k\left(\overline{u_j'u_m'}\varepsilon_{ikm} + \overline{u_i'u_m'}\varepsilon_{jkm}\right) + S_{user} \qquad (4.19)$$

4.1.3.2 Effect of turbulence on particle motion

Turbulent dispersion of particles can be modeled using either a stochastic discrete-particle approach or a "cloud" representation of a group of particles about a mean trajectory. In the current work, the stochastic tracking approach is used.

In Fluent, the Discrete Random Walk (DRW) model is applied to account for the impact of turbulent fluctuations on the particle motion. Particle trajectories are hereby predicted by integrating the trajectory equations for individual particles based on the instantaneous fluid velocity, $\mu_i = \bar{\mu}_i + \mu_i$, along the particle path. The repeated calculations of a single particle trajectory will show different particle trajectories. However, with sufficient number of calculations (the so-called *number of tries* in FLUENT), a representative turbulent dispersion of the particles can be obtained. To compute a particle trajectory, the random fluctuating velocity component (obtained from a GAUSS distribution) has to be kept constant for a certain time interval. This time interval, the so-called Lagrangian integral time, can be approximated with

$$T_L = C_L \frac{k}{\varepsilon}$$
(4.20)

where the constant c_L has to be determined empirically. The software manual [FLUENT, 2004] suggests

$$T_L \approx 0.15 \frac{k}{\varepsilon}$$
(4.21)

for particle tracking with k-ε turbulence models and

$$T_L \approx 0.30 \frac{k}{\varepsilon}$$
(4.22)

when the RSM approach is applied.

4.1.4 Heat and mass transfer models

In general, there are two drying rate periods, i.e., constant drying rate period (CDRP) and falling drying rate period (FDRP) during droplet drying. CDRP is controlled by mass transfer between the drying medium and the droplet. But FDRP is controlled by the mass diffusion within the droplets/particles. In the following section, the built-in models available in FLUENT will be described and followed by models developed in this study and incorporated into FLUENT.

4.1.4.1 Built-in heat and mass transfer models

Because the heat and mass transfer between droplet and drying medium is very complex, several heat and mass transfer relationships are employed in this thesis. Some changes were made as needed using the User Defined Function (UDF) option.

While the particle temperature T_p is less than the vaporization temperature T_{vap} (defined as the temperature at which the droplet/particle will start to evaporate),

$$T_p < T_{vap} \tag{4.23}$$

the droplet is only heated and no evaporation occurs. The heat balance is as follows

$$m_p C_p \frac{dT}{dt} = hA_p \left(T_g - T_p \right) \tag{4.24}$$

where m_p is mass of the particle (kg); c_p is heat capacity of the particle (J/kg·K); A_p is the surface area of the particle (m^2); T_g is the local temperature of the hot medium (K); h is the convective heat transfer coefficient($W/m^2 \cdot K$). The heat transfer coefficient, h, is evaluated using the correlation of Ranz and Marshall [1952a and 1952b]:

$$Nu = \frac{hd_p}{k_g} = 2.0 + 0.6 \mathrm{Re}_d^{1/2} \mathrm{Pr}^{1/3} \tag{4.25}$$

where d_p is the particle diameter(m); k_p is the thermal conductivity of the hot medium ($W/m^2 \cdot K$); Re_d is the Reynolds number based on the particle diameter and the relative velocity; Pr is the Prandtl number of the hot medium($c_p \mu / k_g$).

When the temperature of the droplet exceeds the vaporization temperature, T_{vap}, and continues until the droplet reaches the boiling point, T_{bp}, droplets are assumed to start to evaporate. During this period, the rate of vaporization is given by

$$J_i = k_c (C_{d,s} - C_g) \tag{4.26}$$

where J_i is the molar flux of vapor($kmol/m^2 \cdot s$); k_c is the mass transfer coefficient(m/s); $c_{d,s}$ is the vapor concentration at the droplet surface($kmol/m^3$); c_g is the vapor concentration in the bulk gas($kmol/m^3$); $c_{d,s}$ and c_g are defined as

$$C_{d,s} = \frac{p_{sat}\left(T_p\right)}{RT_p} \tag{4.27}$$

$$C_{d,s} = X_i \frac{\left(p_{op}\right)}{RT_g} \tag{4.28}$$

where $p_{sat}(T_p)$ is the saturated vapor pressure at the particle droplet temperature (Pa); R is the universal gas constant $(J/mol \cdot K)$; X_i is the local bulk mole fraction of species I; p_{op} is the operating pressure (Pa). The mass transfer coefficient in equation (4.26) is calculated from the Nusselt correlation [Ranz and Marshal, 1952a and 1952b]:

$$Nu_{AB} = \frac{h_c d_p}{D_m} = 2.0 + 0.6 \, \text{Re}_d^{1/2} \, Sc^{1/3} \qquad (4.29)$$

where D_p is the diffusion coefficient of vapor in the bulk(m^2/s) and Sc is the Schmidt number $(\mu/\rho D_m)$.

The heat transfer between the droplet and the hot gas is updated according to the heat balance relationship given as follows

$$m_p c_p = \frac{dT_p}{dt} = hA_p \left(T_g - T_p \right) + \frac{dm_p}{dt} h_{fg} \qquad (4.30)$$

where h_{fg}= latent heat (J/kg); $\frac{dm_p}{dt}$ rate of evaporation (kg/s).

The third period, called droplet boiling, is applied to predict the convective boiling of a discrete phase droplet when the temperature of the droplet has reached the boiling point and while the mass of the droplet exceeds the non-volatile fraction. The boiling rate equation is [Kuo, 1986, FLUENT, 2004]:

$$\frac{d\left(d_p \right)}{dt} = \frac{4k_g}{\rho_p c_{p,d} d_p} \left(1 + 0.23\sqrt{\text{Re}_d} \right) \ln \left[1 + \frac{c_{p,d} \left(T_g - T_p \right)}{h_{fg}} \right] \qquad (4.31)$$

where $c_{p,g}$ is the heat capacity of the gas (J/kg·K); ρ_p is the droplet density (kg/m^3); k_c is the thermal conductivity of the gas (W/m·K). The droplet is assumed to stay at constant temperature during this period.

After the volatile fraction reaches the required residual volatile fraction, the particle is treated as an inert particle. It means that the particle will be kept to be heated by the surrounding hot gas and no further evaporation occurs.

4.1.4.2 Proposed modified drying kinetics model

In CDRP, the equation (4.26) still is used to calculate the drying/evaporation rate. When the moisture concentration is reduced to the critical moisture in the particles, the FDRP starts. However, if the particle remains spherical in shape, the

governing equation in the falling drying rate period (FDRP) subject to assumptions started earlier is written as a diffusion process as follows:

$$\frac{dC}{dt} = D_p \left(\frac{\partial^2 C}{\partial r^2} + \frac{2}{r} \frac{\partial C}{\partial r} \right)$$ (4.32)

The boundary conditions are:

$$C(r,0) = C_{cr} \quad \text{at} \quad t = 0 \quad \text{and} \quad 0 \leq r \leq R;$$

$$\frac{\partial C(0,t)}{\partial r} = 0 \quad \text{at} \quad r = 0$$ (4.33)

At the droplet surface, Furuta et al. [1994] suggested the boundary condition as

$$-D_p \frac{\partial C(R,t)}{\partial r} = \psi k_c \left(P_s - P_g \right) \quad \text{at} \quad r = R;$$ (4.34)

where ψ is certain function of water concentration in droplet.

Unfortunately, without access to the source code it is not possible to directly incorporate equation (4.32) within FLUENT. A new drying model is therefore developed here to circumvent this problem. The plot of the normalized drying rate ($J//J_c$) versus normalized free moisture content $[(X - X^*)/(X_c - X^*)]$ called the characteristic drying rate curve, can be assumed to be nearly independent of the drying conditions [Mujumdar et al., 2000]. Such a characteristic drying rate curve is illustrated in Figure 3.1. Thus, if the constant rate-drying rate can be estimated and the equilibrium moisture content data are available, then the falling rate curve can be estimated using this simplified method.

In this work, the constant drying rate is estimated using the following computation:

$$J_c = \frac{h_c \left(T_g - T_w \right)}{\lambda M_w}$$ (4.35)

while the convective heat transfer coefficient h_c is calculated from equation (4.25)

For computation of the drying rate during the falling rate period, equation (4.26) is still used and re-formulated as

$$J_f = k_c \left(\frac{G}{RT_p} - X_i \frac{p_{op}}{RT_g} \right)$$ (4.36)

while the mass transfer coefficient k_c is calculated using equation (4.37)

$$Sh = \frac{k_c d_p}{D_p} = 2.0 + 0.6 \, \mathrm{Re}^{1/2} \, Sc^{1/3} \qquad (4.37)$$
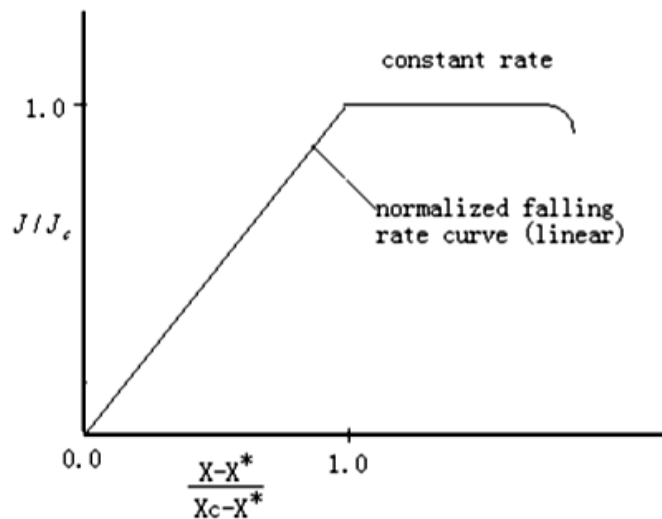
Figure 4.1 Characteristic drying curve.

So, based on the modeled drying rate curve for the falling rate period, the relationship between (J_f/J_c) and $[(X - X^*)/(X_c - X^*)]$ can be obtained. Thus, "pseudo-pressure" G can be computed from the moisture content of the droplet estimated at each computing time step. It can be directly and readily input into FLUENT using its user-define-function (UDF) capability. Note that 'G' is only a mathematical artifact to introduce our model into FLUENT without the need to access the source code.

4.1.5 Coupling between the discrete and continuous phases

Basically, FLUENT solves the conservation equation for mass, momentum and other scalars (e.g. turbulence parameters) as discussed in the earlier part of this chapter. The coupled computation procedure is shown in Figure 4.2.

The last term, F_i, in equation (4.2) describes external body forces, e.g. interaction forces of a dispersed phase (particles) on the continuous phase (fluid). It can be computed as

$$F_i = \sum \left[\frac{18\mu C_D \, \mathrm{Re}}{24\rho_p d_p^2} (u_p - u) + F_{other} \right] \dot{m}_p \Delta t \qquad (4.38)$$

where μ is the dynamic viscosity of the fluid, ρ_p is the density of the droplet/particle, d_p is the diameter of the particle, Re is the relative Reynolds number, u_p is the velocity of the particle, u is the velocity of the fluid, C_D is drag coefficient, $\dot{m}_p$ is mass flow rate of the particles, Δt is time step, F_{other} is other interaction forces. This is the momentum transfer from the continuous phase to the discrete phase.
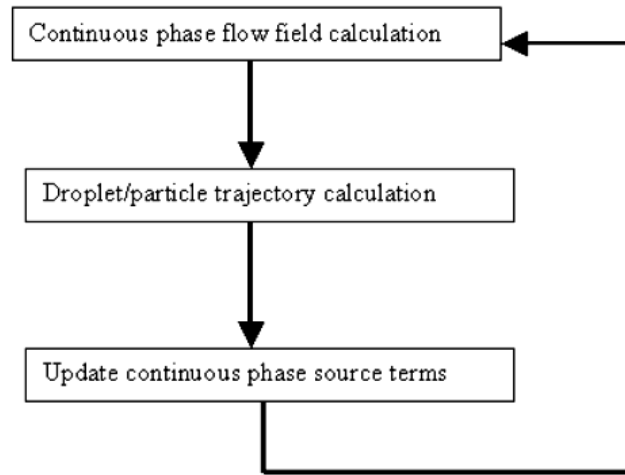
Figure 4.2 Coupled computation procedure in FLUENT

On the other hand, the heat transfer from the continuous phase to the discrete phase is computed by

$$Q = \left[\frac{\bar{m}_p}{m_{p,0}} c_p \Delta T_p + \frac{\Delta m_p}{m_{,0}} \left(-h_{fg} + \int_{T_{ref}}^{T_p} c_{p,i} dT \right) \right] \tag{4.39}$$

where $\bar{m}_p$ is average mass of the particle in the control volume (kg), $m_{p,o}$ is initial mass of the particle (kg), c_p is heat capacity of the particle (J/kg·K), ΔT_p is temperature change of the particle in the control volume(K), Δm_p is change of the mass of the particle in the control volume(kg), h_{fg} is latent heat of volatiles evolved (J/kg), $c_{p,i}$ is heat capacity of the volatiles evolved (J/kg·K), T_p is temperature of the particle upon exit of the control volume (K), T_{ref} is reference temperature for enthalpy (K), $\dot{m}_{p,0}$ is initial mass flow rate of the particle injection tracked (kg/s). It (Q) appears as a source or sink of energy in the continuous phase energy balance.

The mass transfer from the discrete phase to the continuous phase is computed simply as

$$M = \frac{\Delta m_p}{\Delta m_{p,0}} \dot{m}_{p,0} \tag{4.40}$$

This appears as a source of mass in the continuous phase continuity equation.

4.1.6 Solver

In general, the solution step of a CFD problem is carried out by FLUENT in two steps:
- Discretisation: Integration of the governing equations for conservation of mass and momentum, and other scalars (e.g. turbulence parameters) on a cell (= control volume) yielding a set of mathematical expressions for the dependent variables, such as velocity, pressure etc. The second upwind method is used in the following computation.
- Linearization: The above-obtained set of mathematical expressions has to be linearised and solved to update the dependent variables in the control volume (cells).

Starting with an initial guessed solution – provided by the user – this solution procedure is repeated until the pre-set convergence criteria are met and a final solution is obtained via an iterative process. The solution history can be monitored by plotting the sum of the residuals for each dependent variable at the end of each iteration. For a converged solution, the residuals should be a small value (so-called *round off*). In this study a segregated solver with implicit linearization has been applied.

The convergence criteria, main boundary conditions and particle/wall interaction are discussed in Appendix A.

4.1.7 Explanation of Relative Humidity Calculation

The relative humidity (ψ) of the outlet gas (actual vapor pressure (p_v) divided by the saturation vapor pressure) needs to be calculated first, from the gas temperature (T_{Go}) and the gas humidity (Y_o).

$$\psi = \frac{p_v}{p_{vsat}} \tag{4.41}$$

The saturation vapor pressure (p_{vsat}) is the maximum vapor pressure at the outlet gas temperature (T_{Go}), and this vapor pressure may be calculated using the Antoine equation. For water, one version of the Antoine equation is:

$$p_{vsat}(Pa) = 133.3 \exp\left(18.3036 - \frac{3816.44}{T_{po}(°C) + 229.02}\right) \tag{4.42}$$

The actual vapor pressure (p_v) may be related to the outlet gas humidity (Y_o) by

$$Y = 0.622 \frac{p_v}{P_{atm} - p_v} \qquad (4.43)$$

Why? Should a mixture of m_G kg of air and m_v kg of water vapor behave as an ideal gas, one has

$$p_G V = \frac{m_G}{M_G} RT \qquad (4.44)$$
$$p_v V = \frac{m_v}{M_v} RT$$

in which p_G and p_v are the partial pressure of air and water, respectively, m_G and m_v are the molecular weights of air and water, respectively, R is the gas constant and T is the absolute temperature. These pressures may be added together to give the total pressure, P_{atm}:

$$p_G + p_v = P_{atm} \qquad (4.45)$$
$$p_G = P_{atm} - p_v$$

Back substituting into Equation 4.44 gives:

$$(P_{atm} - p_v)V = \frac{m_G}{M_G} RT \qquad (4.46)$$
$$p_v V = \frac{m_v}{M_v} RT$$

The ratio of m_v to m_G is the gas humidity, Y_o, so

$$Y_0 = \frac{M_v}{M_G} \frac{p_v}{P_{atm} - p_v} \qquad (4.47)$$

as required.

Rearranging Equation 4.43 to calculate the actual vapor pressure (p_v) from the gas humidity (Y_o) gives:

$$p_v = \frac{(Y_0/0.622)P_{atm}}{[1+(Y_0/0.622)]} \tag{4.48}$$

Equations 4.40, 4.43 and 4.48 give the relative humidity (ψ) from the gas temperature (T_{Go}) and the gas humidity (Y_o). This relative humidity, together with the gas and solids temperatures ($T_{So} = T_{Go}$), is used to estimate the equilibrium moisture content (X_{emc}), which is an estimate of the outlet moisture content (X_o). There are different equations for the equilibrium moisture content for different materials. For skim milk powder, one sorption isotherm is:

$$X_0 = X_{emc} = 0.1499\exp[-2.306\times10^{-3}(T_{So}+273.15)\cdot\ln(\frac{1}{\psi})] \tag{4.49}$$

CHAPTER V

COMPUTATIONAL FLUID DYNAMICS (CFD) MODEL OF SPRAY DRYERS

5.1 Governing equations

Form chapter 4, conservation of mass and momentum are shown in the general form of spray dryers. The theoretical equations of this work have been proposed in this chapter.

For continuous phase (air);

Continuity equation:

$$\frac{\partial \rho}{\partial t} + \frac{\partial}{\partial x}(\rho u_x) + \frac{\partial}{\partial r}(\rho u_r) + \frac{\rho u_r}{r} = S_m \tag{5.1}$$

where ρ represents density of fluid and u_x and u_r are velocities in axial and redial directions respectively. The subscripts of x and r refer to axial and redial directions. Also S_m is the source term of droplet phase.

Momentum equation:

Axial momentum:

$$\frac{\partial}{\partial t}(\rho v_x) + \frac{1}{r}\frac{\partial}{\partial x}(\text{r}\,\rho u_x u_r) + \frac{1}{r}\frac{\partial}{\partial r}(\text{r}\,\rho u_x u_r) = -\frac{\partial P}{\partial x} + \frac{1}{r}\frac{\partial}{\partial r}\left[r\mu\left(2\frac{\partial u_x}{\partial x} - \frac{2}{3}(\nabla \cdot u)\right)\right]$$
$$+ \frac{1}{r}\frac{\partial}{\partial r}\left[r\mu\left(\frac{\partial u_r}{\partial r} + \frac{\partial u_r}{\partial x}\right)\right] + F_x \tag{5.2}$$

Radial momentum:

$$\frac{\partial}{\partial t}(\rho u_r) + \frac{1}{r}\frac{\partial}{\partial x}(\text{r}\,\rho u_x u_r) + \frac{1}{r}\frac{\partial}{\partial r}(\text{r}\,\rho u_r u_r) = -\frac{\partial P}{\partial x} + \frac{1}{r}\frac{\partial}{\partial r}\left[r\mu\left(\frac{\partial u_r}{\partial x} + \frac{\partial u_x}{\partial r}\right)\right]$$
$$+ \frac{1}{r}\frac{\partial}{\partial r}\left[r\mu\left(2\frac{\partial u_r}{\partial r} - \frac{2}{3}(\nabla \cdot u)\right)\right] - 2\mu\frac{u_r}{r^2} + \frac{2}{3}\frac{\mu}{r}(\nabla \cdot u) + F_r \tag{5.3}$$

where P is the pressure, μ is viscosity of fluid. F_x and F_r are the forces acting in axial and redial directions. The velocity gradient in momentum equations are described by following equation.

$$\nabla \cdot u = \frac{\partial u_x}{\partial x} + \frac{\partial u_r}{\partial r} + \frac{u_r}{r}$$

(5.4)

The energy conservation equation for gas can be written as

$$\frac{\partial}{\partial x}(\rho_g u q) + \frac{1}{r}\frac{\partial}{\partial r}(r \rho_g v q) = \frac{\partial}{\partial x}\left[\left(\mu_L + \frac{\mu_T}{\sigma_h}\right)\frac{\partial q}{\partial x}\right] + \frac{1}{r}\frac{\partial}{\partial r}\left[\left(\mu_L + \frac{\mu_T}{\sigma_h}\right)r\frac{\partial q}{\partial r}\right] + M_h$$

(5.5)

where, u are the average axial velocity of gas, respectively; q is the enthalpy of gas; M_h is the rate of heat transfer between the droplets and the gas. The laminar viscosity of the fluid is μ_L and the turbulent viscosity is described by μ_T.

For disperse phase (droplet);

Based on the solution obtained for the flow field of the continuous phase, using an Euler-Lagrangian approach we can obtain the particle trajectories by solving the force balance for the particles taking into account the discrete phase inertia, aerodynamic drag, gravity g_i and further optional user-defined forces F_{xi}.

Continuity equation:

$$\frac{\partial u_{pi}}{\partial x} = C_D \frac{18\mu}{\rho_p d_p^2} \frac{Re}{24}(u_i + u_{pi}) + g_i \frac{\rho_g - \rho}{\rho_g} + F_{xi}$$

(5.6)

with particle velocity u_{pi} and fluid velocity u_i in direction, particle density ρ_p , gas density ρ_g , particle diameter d_p and relative Reynolds number

$$Re = \frac{\rho d_p |u_{pi} - u_i|}{\mu}$$

(4.7a)

and drag coefficient

$$C_D = a_1 + \frac{a_2}{Re} + \frac{a_3}{Re^2}$$

(4.7b)

where a_1, a_2 and a_3 are constants [Fluent, 2004].

The heat transfer between the droplet and the hot gas is updated according to the heat balance relationship given as follows

$$m_p c_p = \frac{dT_p}{dt} = hA_p\left(T_g - T_p\right) + \frac{dm_p}{dt}h_{fg}$$

(4.30)

where h_{fg}= latent heat (J/kg); $\frac{dm_p}{dt}$ rate of evaporation (kg/s). T_g is the local temperature of the hot medium (K) and T_p is the particle temperature.

Boundary conditions

Table 5.1 Boundary condition (Kieviet, 1997)

PARAMETERS	VALUE
Inlet Air	
Air inlet temperature (K)	468
Air mass flow rate (kg/s)	0.336
Air total velocity (m/s)	9.15
Outlet Condition	
Outflow & reference pressure (Pa)	-100
Turbulence Inlet Conditions	
Turbulence k-value (m^2/m^2)	0.027
Turbulence ε-value (m^2/m^3)	0.37
Liquid Spray From Nozzle	
Liquid feed rate or spray rate (kg/s)	0.0139
Feed temperature (K)	300
Spray angle (∘)	76
Minimum droplet diameter (μm)	10
Maximum droplet diameter (μm)	138
Average minimum droplet diameter (μm)	70.5
Particle velocity at nozzle (m/s)	59
Rosin-Rammier parameter	2.05
Chamber Wall Condition	
Chamber wall thickness (mm)	0.002
Wall material	Steel
Overall wall heat transfer coefficient (W/m^2.K)	3.5
Air temperature outside wall (K)	300
Interaction between wall and particle	escape

In the simulation of spray drying, the main assumptions made are:

(A) Discrete phase in continuous phase is sufficiently dilute. In practice, the volume fraction of discrete phase to the continuous phase should be less than 2%. Thus, the particle-particle interactions and the effects of the particle volume fraction on the gas phase are negligible.

(B) Agglomeration and break-up among the droplets or particles are neglected.

(C) The droplets/particles are always assumed to be spherical. During droplet drying, the spherical shape is always assumed.

(D) Constant drying rate period and 1st step of drying (no mass transfer) of this system is always assumed.

(E) No slip condition at wall as the result of velocity at wall equal zero is assumed.

5.2 Validation model

This chapter presents the prediction results for a co-current spray dryer fitted with a pressure nozzle using both 2D CFD models. Some of these results are validated using the published data of Kieviet [1997]. Parametric studies were carried out as well.

5.2.1 Problem description

Figure 5.1 shows the tested spray dryer geometry used in this work which is the same as that studied by Kieviet (1997). The chamber is a cylinder-on-cone vessel, 2.215 m in diameter and with a cylinder top section, height of 2.0 m and the bottom cone with 1.725 m height. The angle of the cone is 60◦. Hot air is blown from the ceiling of the drying chamber through an annular tube which has an outer diameter of 495.6 mm and an inner diameter of 411.6 mm. The pressure nozzle is located at the center of drying chamber, 229 mm away from the flat ceiling of chamber. There is an exit tube for the exhaust air conveying the dried particles at the center of the cone. The outlet diameter is 172 mm.
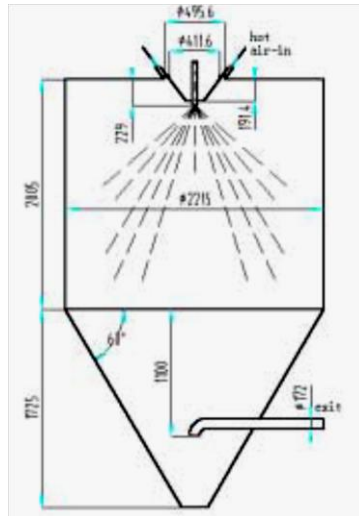
Figure 5.1 Tested geometry with dimensions in mm (Kieviet, 1997)

5.3 Validation cases

The simulations are performed for steady state operations. The 2D axi-symmetrical model which is same as the model used by Kieviet (1997) was selected for simulation. Square grids were used for the drying chamber. The results for airflow patterns and temperature fields were similar when different mesh sizes were used. Hence, the results are considered to be grid-independent. The number of grid point used for the geometry tested is 3765.

5.3.1 Boundary conditions

Cases A and B are defined as the spray dryer without any spray and with spray.

Inlet air: The velocity of drying air is 7.36 m/s for the case without spray and 9.15 m/s with spray. Temperature of the air at inlet is set at 468 K and its relative humidity is 75% at 25 ºC.

Outlet conditions: The outlet pressure is set at –100 Pa, i.e., a fan is assumed to draw air out from the drying chamber.

Chamber wall conditions: According to the options that could be selected for the present work in the FLUENT code, when a droplet/particle hits the wall of the drying chamber, it can be assumed to be "trapped" or "escaped" or "reflected" by the wall. Under the "trap" condition, all non-volatile material is "lost" from the calculation at the point of impact with the wall. The volatile material present in the trapped particle/droplet is assumed to be released to the gas phase at this point. However, under the "escape" condition, the particles are removed from the calculation at the point of impact with the wall. According to the "reflect" condition, the particles rebound off the wall with a change in its momentum as defined by the

coefficient of restitution. In this validation case, the "escape" boundary condition is used.

The overall heat transfer coefficient from the wall to the outside of the drying chamber is estimated to be 3.5 W/m^2.K and the chamber wall is assumed to be made of 2 mm thick stainless steel. This coefficient value is obtained by fitting published measurement results (Kieviet, 1997) with a simulation carried out with spray.

Spray from nozzle: An "injection" condition is defined here to specify the spray with a given droplet size distribution. The spray mass flow rate is 59 kg/h (0.013889kg/s) with 42.5% solids content. The feed temperature is set at 300 K. The spray angle is assumed to be 760. The droplet size distribution is such that 0.10 μm is the minimum droplet diameter and 0.138 μm is the maximum droplet diameter with an average droplet diameter D of 70.5 μm. The droplet diameter distribution is modeled using a Rosin-Rammler curve with these parameters and the spread parameter equal to 2.05 (Kieviet, 1997). The droplet velocities at nozzle exit are fixed to be 59 m/s (Kieviet, 1997). In order to simplify the calculation, the feed physical properties are assumed to be those of water, except that the volatile content is allowed to change as drying proceeds.

Turbulence model: For the 2D-axisymmetric model, the standard k-ε turbulence model was used. Because there is no swirling flow in the drying chamber, the standard k-ε model is expected to be an appropriate choice for simulating such a flow (Oakley, 1994). The turbulent kinetic energy at the inlet was set at 0.027 m^2/s^3 and the energy dissipation rate at the inlet to be 0.37 m^2/s^3 which are the same values as those used by Kieviet (1997). For tracking the droplets, the turbulent stochastic model (TSM) option was used. Turbulent stochastic tracking of droplets allows for the effect of random velocity fluctuations of turbulence on particle dispersion to be accounted for in the prediction of particle trajectories.

5.3.2 Comparison between measurements and predictions

The predicted velocity profiles for Case A and measured results by Kieviet (1997) at different levels in the drying chamber are shown in Figure 5.2. Figure 5.2 shows that the predicted velocities agree well with the measured results. It is seen that there is a non-uniform velocity distribution in the core region of the chamber. The highest velocity magnitude is about 7.0 m/s at the 0.30 m level. The velocity magnitude is reduced as the air goes into the chamber further due to the expanding area.
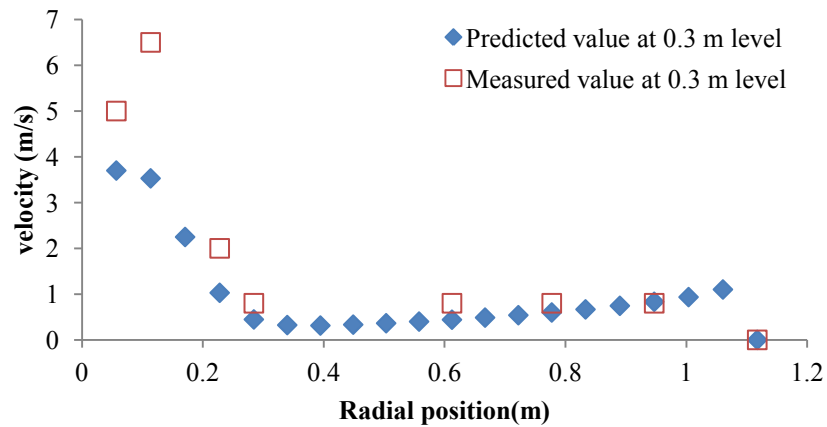
Figure 5.2a Comparison of velocity profiles between prediction and Kieviet's measurement (1997) at 0.3 m and no spray condition
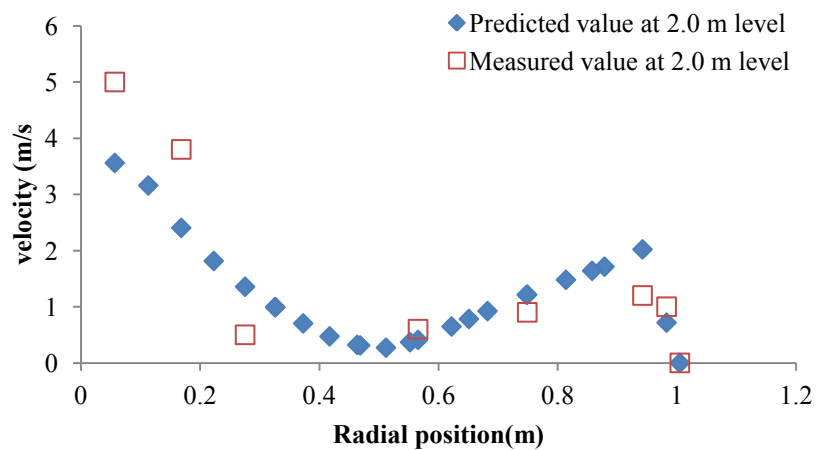

Figure 5.2b Comparison of velocity profiles between prediction and Kieviet's measurement (1997) at 2.0 m under no spray condition

Figure 5.3 shows the predicted temperature profile for Case B and the measured data by Kieviet (1997) at different levels in the drying chamber. It is found that the predicted results agree well with the measured results. The simulation results provide details of the temperature field at different levels and anywhere inside the chamber. The measurement results however do not give such detail because of the limited number of measurement points.
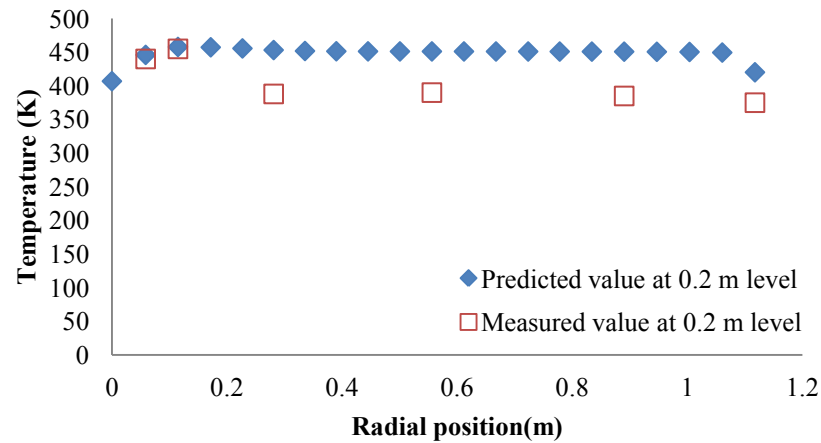
Figure 5.3 Comparison of temperature profiles between prediction and Kieviet's measurement (1997) at 0.2 m under spray condition

From the predicted temperature profiles (Figure 5.3), it is observed that the temperatures in the central core up to a radius of 0.1 m are quite different at different levels which are expected as a direct result of drying. There is only a minor radial variation in the gas temperature. The largest temperature changes usually occur at the first level. It is the result of very high heat and mass transfer rates in the nozzle zone due to high relative velocities between the gas and the droplets coupled with large temperature driving forces.

CHAPTER VI

PREDICTION OF WALL DEPOSITION

6.1 Prediction of wall deposition by viscous stress

6.1.1 Boundary conditions

In a co-current spray dryer, feed solution and hot air enter the chamber in the same direction. As a result, the hot air contacts a droplet of feed solution at its maximum moisture content. As the rate of water evaporation is rapid, the air temperature is reduced. Therefore, a final product does not suffer from heat degradation. Figure 6.1 shows the schematic diagram of the spray dryer used in this study.
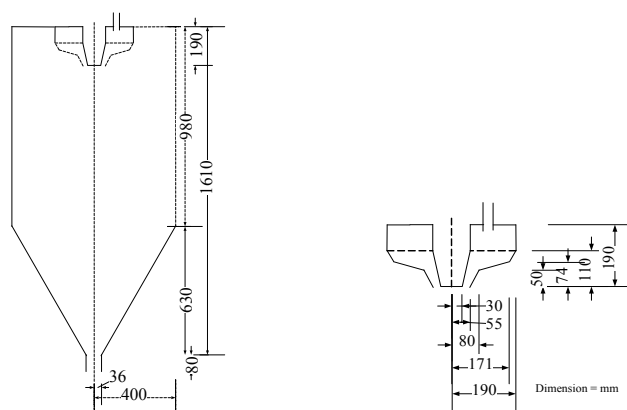

Figure 6.1 Schematic diagram of the spray dryer (Fletcher and Langrish, 2009).

The feed solution consists of anthocyanin spherical particles and water with density of 1,240 kg/m^3 and dynamic viscosity of 3.588×10^{-4} mPa·s. The predicted velocity of droplets is shown in Figure 5.2. It is found that the droplet particle has its maximum velocity near the atomizer region. The particle velocity slightly decreases along the center of the drying chamber. Figure 5.2 also shows the flowing direction of the particle. Three patterns of the droplet direction are observed: (1) the particle falls down along the center and goes out the chamber at the outlet with high velocity because of its less moisture content, (2) some particles hit the conical wall and then fall down along the slope-sided surface at the medium velocity and (3) most of moisture-containing droplets hit the side wall and flow upward to the top of the chamber and then recirculate downward to the bottom with low velocity. The recirculation results in a longer residence time of the droplets with high moisture content. This factor may degrade a quality of the final product if some important nutrient in the producet is sensitive to heat.
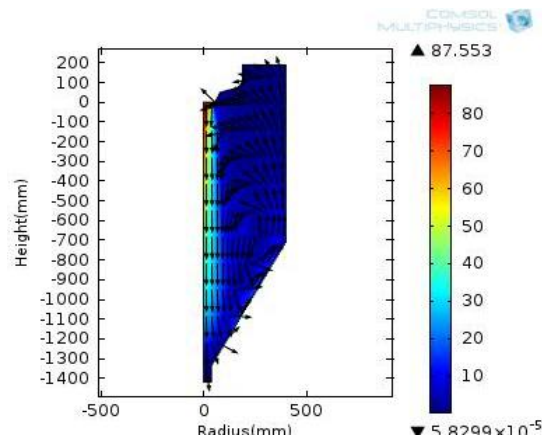
Figure 6.2 Velocity (m/s) of droplets in the spray dryer.

6.1.2 Results and discussion

6.1.2.1 Effect of viscous stress in the axial and radial directions

Figure 6.3 shows the region of velocity field in the radial and axial directions. The results indicate that most droplets with high moisture content hit the conical wall of the chamber with radial and axial- direction forces, resulting from a viscous stress of the droplets. Figure 6.4 shows that the viscous stress in the axial and radial directions. It is found that the viscous stress is dominated by the force in the axial direction. So the droplets are possibly attached at the maximum viscous stress region.
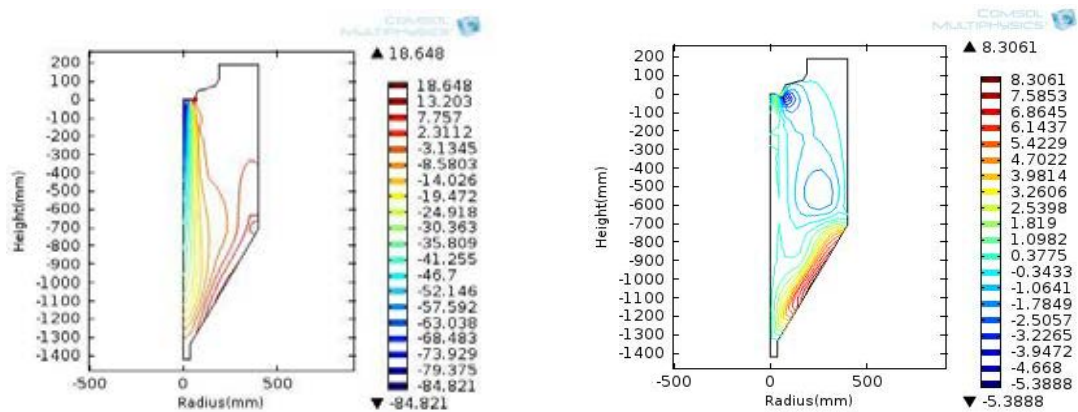

Figure 6.3 Contour plot of the velocity field (m/s) in the radial (left) and axial (right) directions.
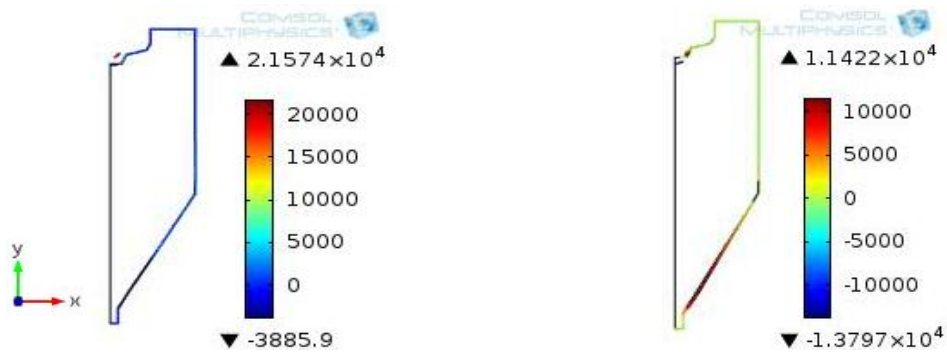
Figure 6.4 Viscous stress (N/m^2) in the radial (left) and axial (right) directions.
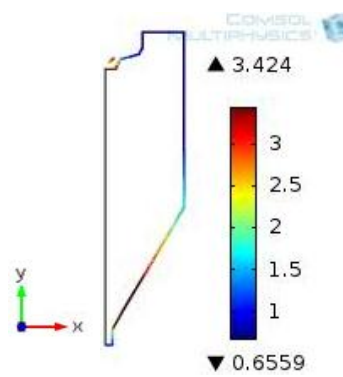

Figure 6.5 Friction velocity (m/s) at the wall chamber.

In general, dry particles absorb moisture and heat from wet and hot particles. As the result, the rebond of these particles tends to be stick. The first layer of sticky particles attaches to the chamble wall with the adhesion of particles to top layer of the wall. The second layer of sticky particles attaches to the first layer of the sticky particles with the cohesion of layer particles and the pattern for the next layers is similar. In order to understand the effect of a wall deposition problem, the friction velocity at the chamber wall is studied. Figure 6.5 indicates that the maximum friction velocity region is at the conical wall, which is the same region as the viscous stress in the axial direction (Figure 6.4).

6.1.2.2 Effect of viscous stress to configuration

The flow pattern of droplets within the spray dryer with different conical wall angles is studied. Figures 6.6 and 6.7 show effect of the conical wall angle on the viscous stress along the axial direction. When the height of side wall and diameter of chamber increase, they decrease the angle of the conical wall. The maximum viscous stress in the axial direction increases as the angle of the conical wall is less than its nominal value. It is found that the droplets hit a conical wall and then move upward to the top or downward to the botton of the chamber with slow velocity and height tangential viscous stress. Thus, the droplets build up on the wall.
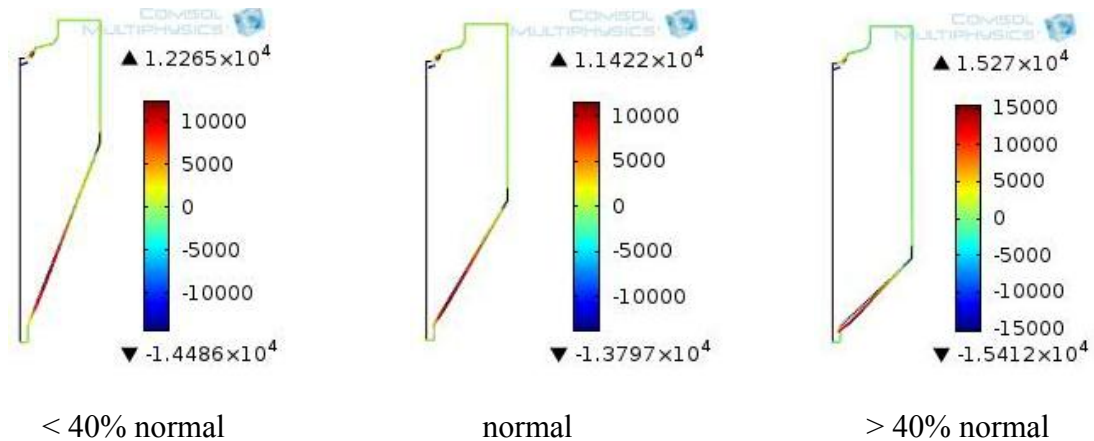
< 40% normal	normal	> 40% normal

Figure 6.6 Comparison of the viscous stress (N/m^2) in the axial direction at different heights of the side wall.

< 25% normal	normal	> 25% normal
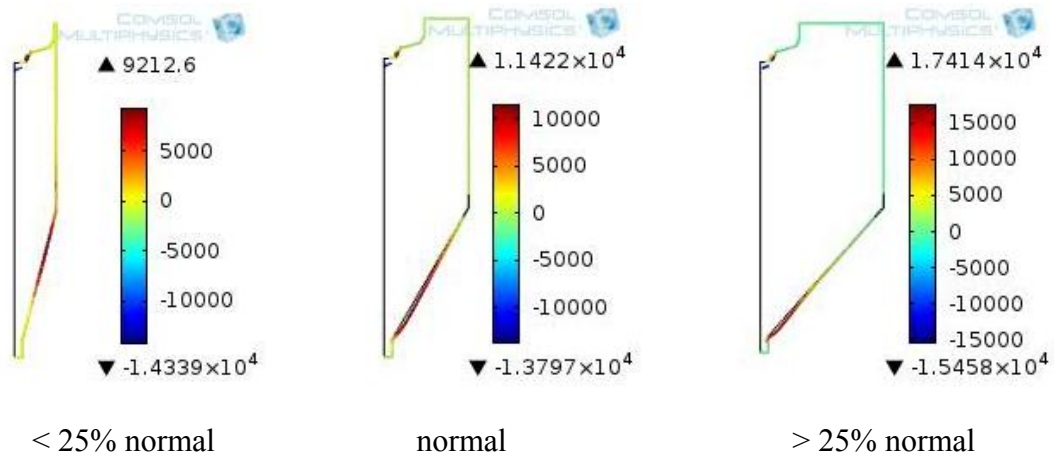
Figure 6.7 Comparison of the viscous stress (N/m^2) in the axial direction at different chamber diameters.

6.1.2.3 Effect of viscous stress to inlet velocity

Effect of inlet fluid velocity on the wall deposition problem is studied. Figure 6.8 shows the viscous stress in the axial direction when the inlet velocity is 80 m/s (nominal flowrate). When the inlet velocity is changed from 60 to 100 m/s, a similar trend is observed.

In addition, the flow fields obtained show a similar trend the maximum viscous stresses at the inlet velocity of 60, 80 and 100 m/s are 6,420, 11,422 and 17,858 N/m^2, respectively. The results show a linear relationship of the inlet velocity of feed droplets and the maximum viscous stresses. The viscous stress increases with increased inlet velocity. Thus, at a higher inlet fluid velocity, the tendency of the droplet to be attached the wall increases due to high adhesive force.
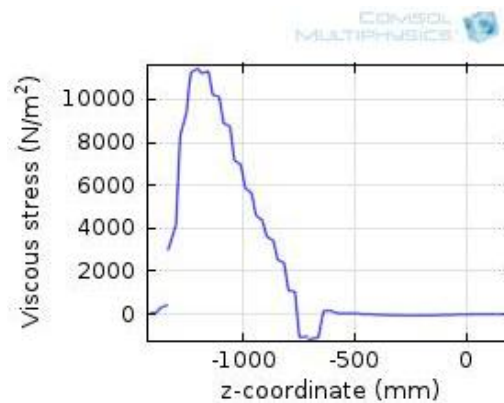
Figure 6.8 Viscous stress (m/s) in the axial direction at the wall chamber (inlet fluid velocity = 80 m/s).

The viscous stress and friction velocity in the axial direction are key factors to explain a wall deposition problem. Droplets are possibly attached to the wall at the position that the viscous stress and friction velocity show their maximum values. The influences of design parameters of the spray dryer and inlet fluid velocity were also studied. When the angle of the conical wall decreases, the maximum viscous stress in the axial direction increases. The viscous stress region at the wall chamber shows a linear relation with the inlet fluid velocity.

This study investigated a turbulent flow behavior within a co-current spray dryer for anthocyanin droplets. The simulation results indicated three flowpatterns; (1) droplets fall down and go out the dryer, (2) droplets hit the conical wall and then fall down along the wall of the chamber and (3) droplets hit and move upward to the top of the chamber at the side wall and then recirculate downward to the bottom.

6.2 Prediction of wall deposition by glass transition temperature and sticky-point concept

Energy leaves the dryer mainly through the cooler, moister, air, also through the solids (which contain some moisture). The outlet solids are close to be in equilibrium with the outlet gas, so the temperature of the gas and the solids may be assumed to be the same and the outlet moisture content of the solids can be assumed to be equal to the equilibrium moisture content of solids in contact with the outlet gas. All the moisture that is evaporated from the solids is taken up by the gas, so a mass balance allows the outlet moisture content of the solids to be related to the outlet humidity of the gas.

The stickiness of powder can be explained by a low glass transition temperature (T_g) of components with low molecular weight. Glass transition temperature (T_g) is a reference parameter to project the spray drying systems and characterize the properties, quality, stability and safety of product. Structural alterations, such as stickiness, agglomeration, caking and crystallization, usually occur in amorphous food powders when stored and processed at temperatures above T_g. Sticky-point temperatures (T_s) have relative with glass transition temperature (T_g) and its can begin 10-20 ℃ above the glass transition temperature (Bhandari, 1997a).

The objective of this study was to spray dry by using various drying agent materials in table 6.1 as a drying aid and characterize the stability of the results by glass transition and sticky curve analysis. It aimed to lay a foundation for industrial development and applications of powdered products.

Table 6.1 glass transition temperature of various food materials

Food materials	T_g (℃)[abs]
Fructose	14
Glucose	31
Galactose	32
Sucrose	62
Maltose	87
Lactose	101
Citric acid	6
Tartaric acid	18
Malic acid	-21
Lactic acid	-60
Maltodextrins	
DE[d]36(MW=550)	100
DE 25(MW=720)	121
DE 20(MW=900)	141
DE 10(MW=1800)	160
DE 5(MW=3600)	188

Food materials (cont.)	T_g (°C)^{abs}
Strach	243
Ice-cream	-34.3
Honey	-42 to -51

6.2.1 Boundary conditions

Spray drying: A spray dryer and operating condition (Chapter 5.3.1) same as that studied by Kieviet (1997) was used in the study. Co-current flow regime and a two-fluid nozzle atomizer were used for the spray drying process. The inlet air temperature was set to 195 °C and the outlet air temperature was set to and maintained at 27 °C.
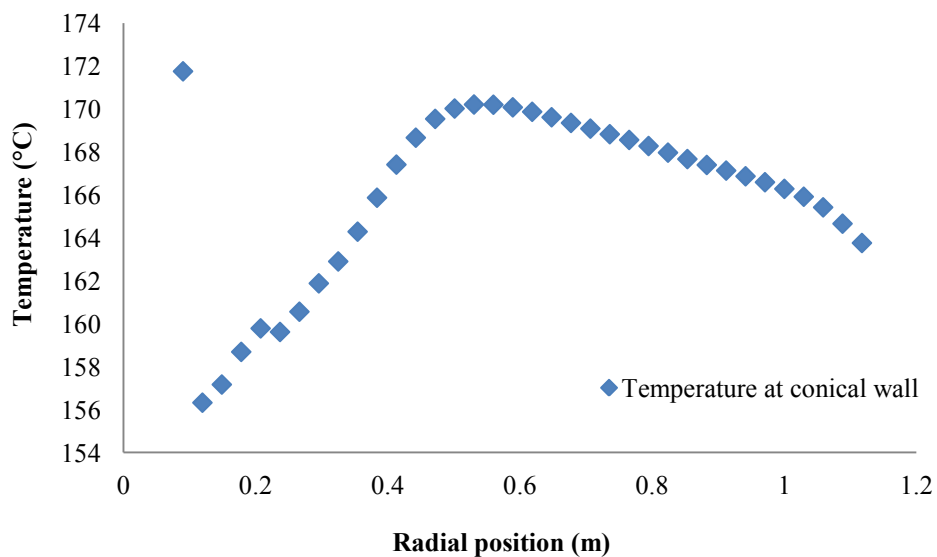
Figure 6.9a Gas temperatures at conical walls.

From this conditions are obtained a gas temperature curve at the conical and cylindrical wall in Figure 6.9. Figure 6.9a shown that temperature at the conical wall near the angle of chamber has higher than near the outlet and temperature at the cylindrical wall near the top of chamber has slightly higher than near the angle of chamber because of a higher heat transfer from hot dried air medium.
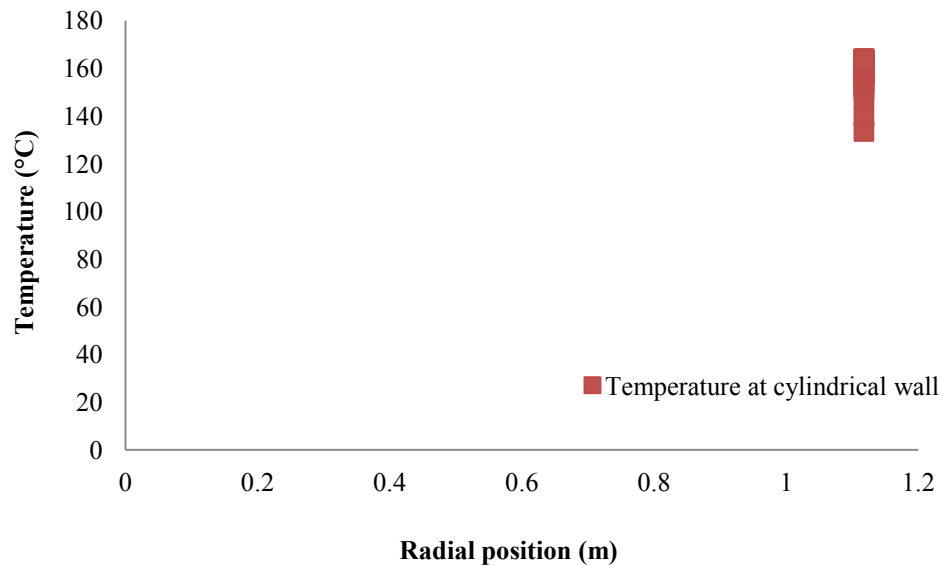
Figure 6.9b Gas temperatures at cylindrical walls.

6.2.2 Results and discussion

6.2.2.1 Effect of drying agent materials

Figures 6.10 to 6.13 are showed effect of the gas temperature on glass transition temperature (T_g) and sticky-point temperature (T_s) at conical and cylindrical wall respectively. Each curves of result have gas temperatures point, sticky-point temperatures and glass transition temperature on each drying agent materials such as maltrodextrins DE[d] 36, DE 25, DE10 and without drying agent material (pure water; T_g = -137 °C). Figure 6.10 and 6.11 indicated that the particles hit the wall in the sticky state and attach on region of walls due to gas temperatures curve are above stickiness temperatures and glass transition temperatures. And particles hit the wall and may be less attach on the wall in Figure 6.13 because the gas temperature is overlap on the stickiness temperature but it is above on the glass transition temperature. So the particles may be in sticky state at the low moisture content. In the other hand, Figure 6.14 gas temperature curve is under both of stickiness temperature and glass transition temperature, it indicated that the particles in this curve are in non-sticky region and state. Not only these particles hit the walls more velocity and every directions but also its not attach the wall. Maltodextrins was able to significantly increase the T_g compared to pure water (Figure 6.10) that agree with Wang and Zhou (2013).
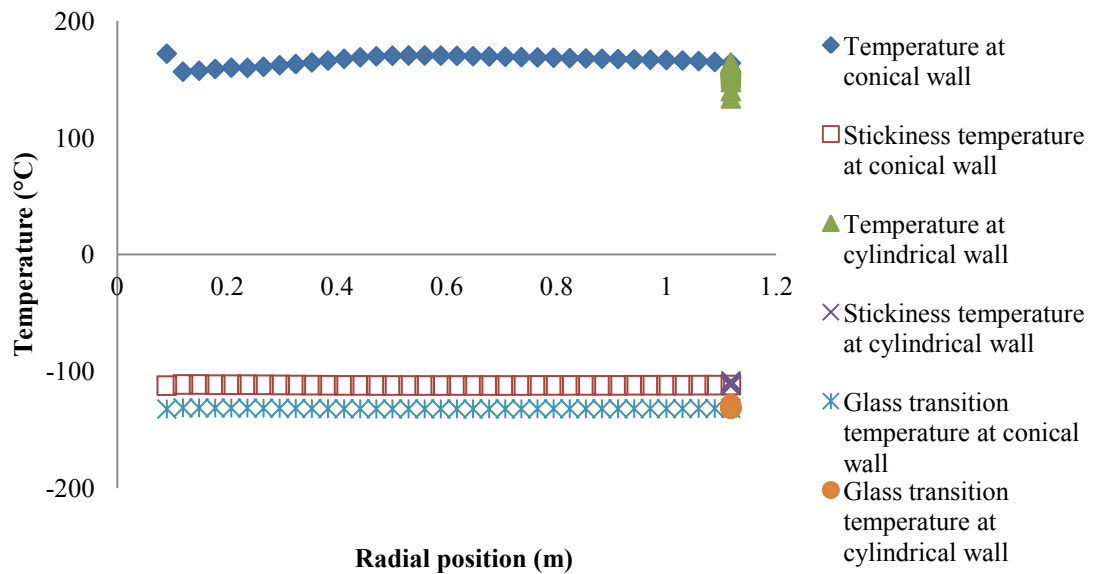
Figure 6.10 Sticky-point curve and gas temperature without drying agent.

6.2.2.2 Effect of maltodextrin DE value

Additives agent materials have been used to produce physical changes in the product, consequently reducing the stickiness and wall deposition in spray drying that maltodextrins are used to drying agent in this study.

The influence of the maltodextrin DE value on the T_g value were significantly shown in Figure 6.10 to 6.13. The predicted results of T_g showed that the maltodextrins with higher DE led to particles with lower glass transition temperatures as shown in Figure 6.10 and 6.11 and increasing the DE value of maltodextrin gave rise to a higher hygroscopicity of the particle containing it. However, the hygroscopicity difference was not significant on low DE value of maltodextrins (Figure 6.12 and 6.13).

T_g increased with increasing molecular weight, maltodextrins were used to improve dehydration characteristics, to decrease stickiness, and to improve product stability. It is popular to incorporate maltodextrins as a carrier in spray drying hygroscopic powders such as fruit juice powders and infant formula. It has significantly increase glass transition temperature (T_g) and reduce hygroscopicity of the final product. And glass transition temperature and sticky-point curve concept are approximated sticky point enough in order to predict a range of simple sticky particles.
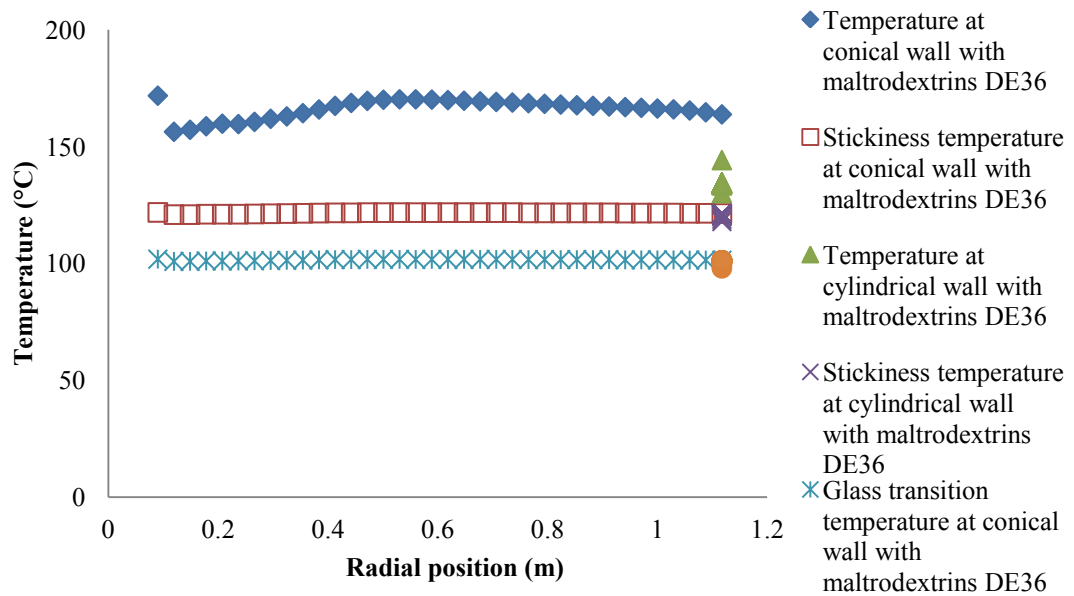
Figure 6.11 Sticky-point curve and gas temperature at wall

with maltrodextrins DE^{d} 36.
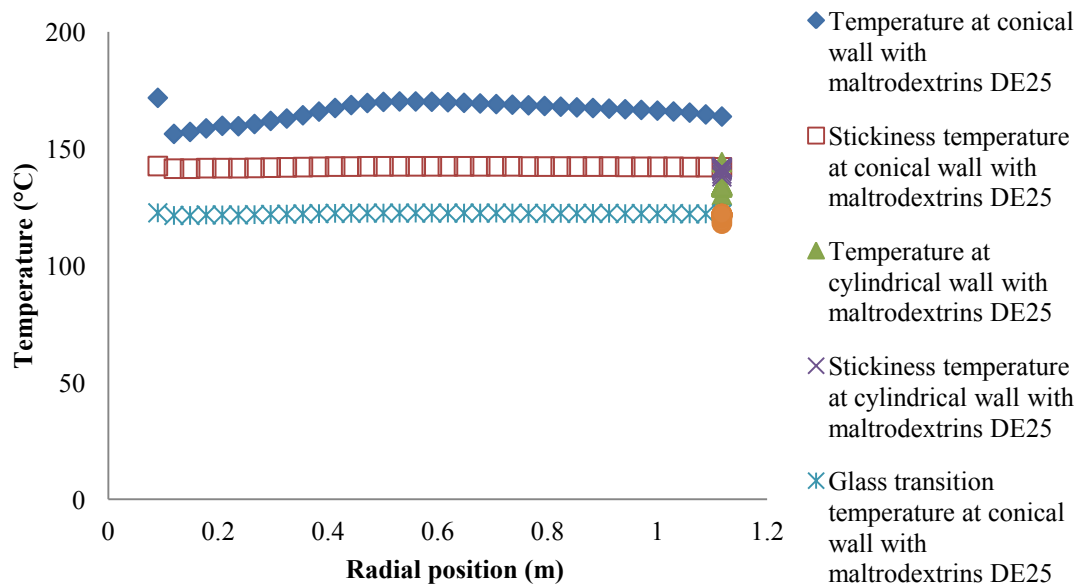
Figure 6.12 Sticky-point curve and gas temperature at wall

with maltrodextrins DE 25.
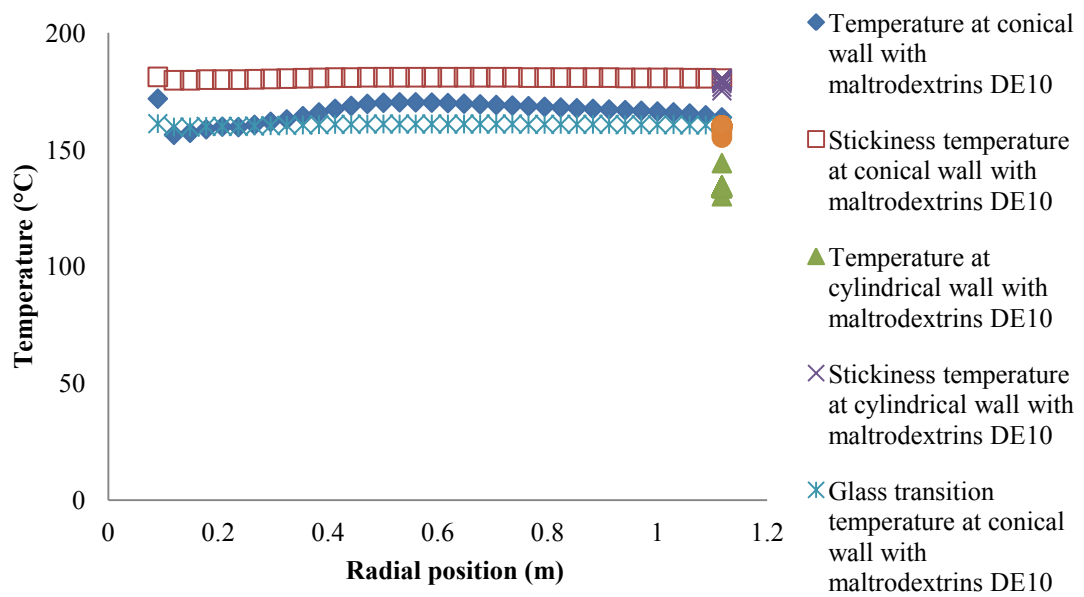
Figure 6.13 Sticky-point curve and gas temperature at wall

with maltrodextrins DE 10.
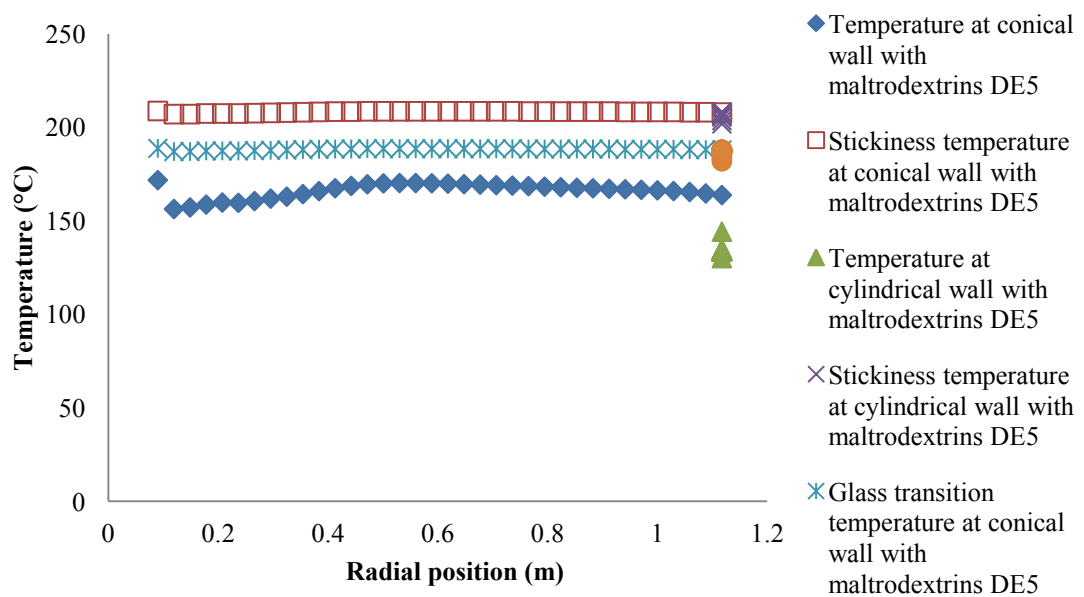
Figure 6.14 Sticky-point curve and gas temperature at wall with maltrodextrins DE 5.

6.2.2.3 Effect of droplet moisture content to glass transition temperature

Figure 6.15 and 6.16 indicated effect of droplet moisture content to glass transition temperature. Humidity of droplet increases, as the result of the glass transition temperature of system decreases.
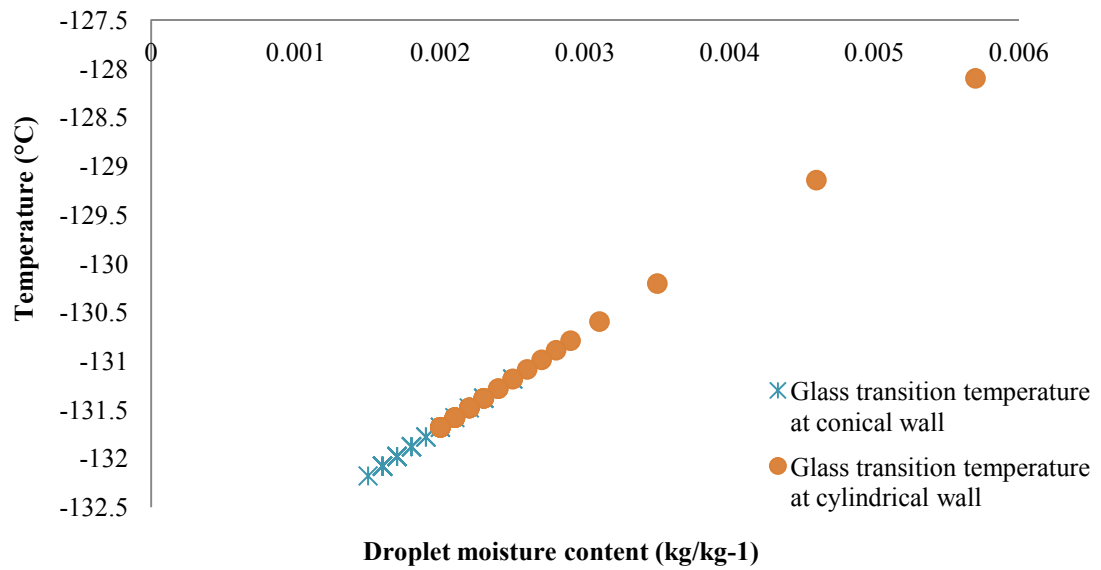
Figure 6.15 Gas transition temperatures and droplet moisture content at wall.
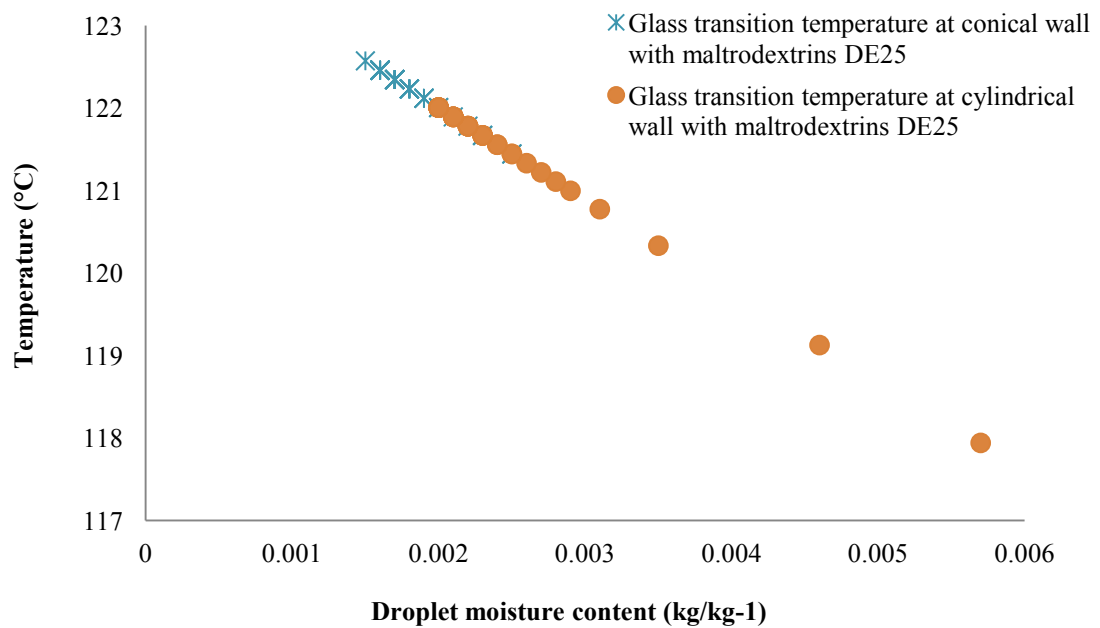
Figure 6.16 Gas transition temperatures and droplet moisture content at wall

with maltrodextrins DE 25.

6.3 Prediction of wall deposition by particle impact position

The knowledge of particle impact position is important for the design and operation of spray dryers as it influences the final product quality. Particle stickiness is related to wall deposition for spray dryers, determining the fate of particles that hit the walls. Whether or not particles hit the wall is a function of the fluid flow patterns in the equipment, and this is an area in which CFD can predict the particle trajectories, so that it is possible to estimate whether the particles hit the walls and the temperatures of such particles. Therefore, a percentage of particles impact position is studied. CFD model use hot dried air and water in the continuous and disperse phase respectively and additional maltrodextrin DE 10. Heat transfer coefficient is 3.5 W/(m^2·K).

6.3.1 Results and discussion

6.3.1.1 Effect of wall temperature range

From CFD solver is obtained a percentage of particle attached the walls chamber via count particles at wall of each temperature range as shown in table 6.1. Figure 6.17 shown that a maximum particle at total wall is 68.571% in 160.0 - 177.5 ◦C temperature range. This temperature range has higher than glass transition temperature, as the results of particles are in a sticky state and attach the walls 68.571%. And 142.5 - 160.0 ◦C range maybe sticky particles because 160.0 ◦C of particles equal to glass transition temperature. Particles are attached on the conical wall more than cylindrical wall as shown in table 6.2. This result is agreed with Kieviet (1997).
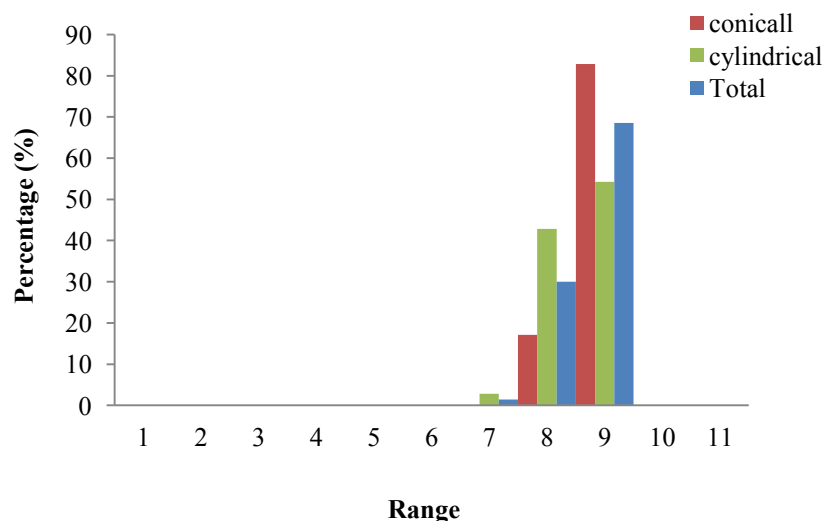
Figure 6.17 Percentage of particles at walls.

Table 6.2 Percentage of particles at walls

RANGE	TEMPERATURE (K)	PERCENTAGE OF PARTICLES (%)			X_0	T_s (°C)	T_g (°C)
		CONICAL WALL	CYLINDRICAL WALL	TOTAL WALL			
1	0.0 - 20.0	0	0	0			
2	20.0 - 37.5	0	0	0			
3	37.5 - 72.5	0	0	0			
4	72.5 - 90.0	0	0	0			
5	90.0 - 107.5	0	0	0			
6	107.5 - 125.0	0	0	0			
7	125.0 - 142.5	0	2.857	1.429	0.0076	172.55	152.55
8	142.5 - 160.0	17.143	42.857	30.000	0.0041	176.65	156.65
9	160.0 - 177.5	82.857	54.286	68.571	0.0022	180.06	160.06
10	177.5 - 468.0	0	0	0			
11	468.0 - 500.0	0	0	0			
TOTAL		100	100	100			

6.3.1.2 Effect of wall heat transfer coefficient

In this part, the effect of wall heat transfer coefficient is studied. Heat transfer coefficient of the wall changes, the temperature of the gas at the wall as the heat transfer coefficient reduction, temperature of the gas at the wall will be higher. On the contrary, heat transfer coefficient increased, as the resulted of a decrease in the temperature of gas at the wall, as shown in Figure 6.18. The heat transfer coefficient is used in 2, 3.5 and 5 W/(m^2·K). Figure 6.19 and 6.20 shown percentage of particle gas temperature at the walls of the heat transfer coefficient is 2 and 5 W/(m^2·K) respectively. The heat transfer coefficient is 2 W/(m^2·K) in table 6.3 indicated that the temperature rage 172.62 - 175.91 ◦C is higher than glass transition temperature. These particles 100 % in this rage are in sticky state and attach the wall 100%. In the other hand, the heat transfer coefficient is 5 W/(m^2·K) in table 6.4 indicated that lower the temperature rage 160 ◦C is under glass transition temperature, particles are not attach the wall. But temperature rage 160.00 - 177.00 ◦C is higher, as the result of these particles attach wall 15.714 %.

A high of heat transfer coefficient useful to decrease the wall temperature for important sugars like Lactose, Maltose and Sucrose that are present in milk and fruit juices. Taking into account the high ratio of milk containing Lactose, the distribution of wall temperature indicates that there is low stickiness on most parts of the dryer wall.
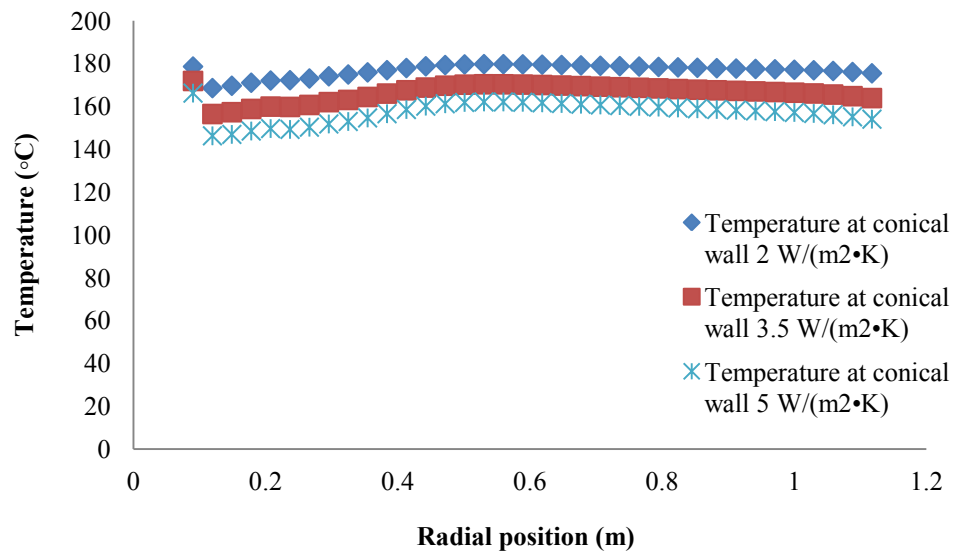
Figure 6.18 Temperature at wall with various heat transfer coefficients.
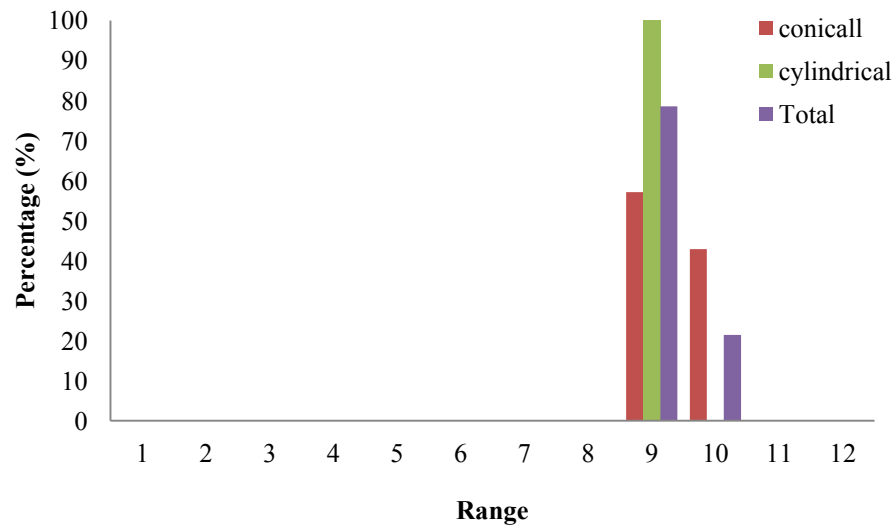
Figure 6.19 Percentage of particles at walls on heat transfer coefficient 2 W/(m²·K)

Table 6.3 Percentage of particles at walls on heat transfer coefficient 2 W/(m²·K)

RANGE	TEMPERATURE (K)	PERCENTAGE OF PARTICLES (%)			X_0	T_s (°C)	T_g (°C)
		CONICAL WALL	CYLINDRICAL WALL	TOTAL WALL			
0	0.00 - 161.11	0	0	0			
1	161.11 - 162.75	0	0	0			
2	162.75 - 164.40	0	0	0			
3	164.40 - 166.04	0	0	0			
4	166.04 - 167.68	0	0	0			
5	167.68 - 169.33	0	0	0			
6	169.33 - 170.97	0	0	0			
7	170.97 - 172.62	0	0	0			
8	172.62 - 174.26	57.143	100	78.571	0.0014	181.23	161.23
9	174.26 - 175.91	42.857	0	21.429	0.0013	181.37	161.37
10	175.91 - 177.56	0	0	0			
TOTAL		100	100	100			
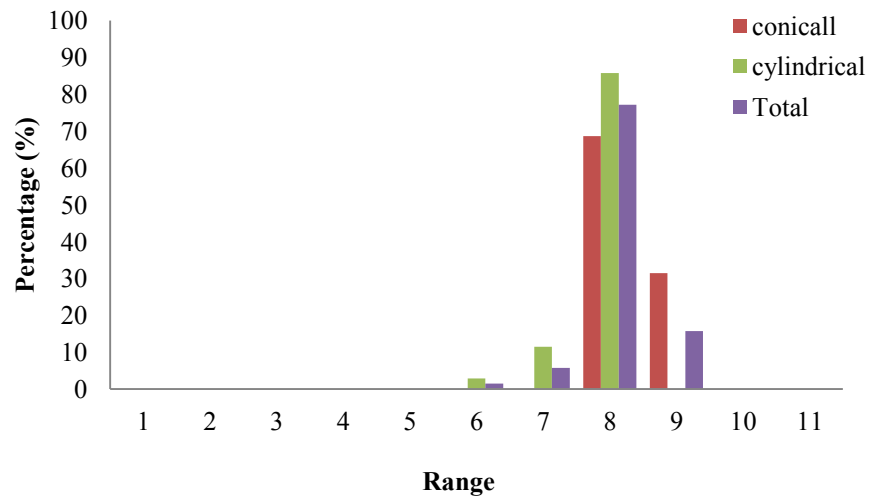
Figure 6.20 Percentage of particles at walls on heat transfer coefficient 5 W/(m^2·K)

Table 6.4 Percentage of particles at walls on heat transfer coefficient 5 W/(m^2·K)

RANGE	TEMPERATURE (K)	PERCENTAGE OF PARTICLES (%)			X_0	T_s (°C)	T_g (°C)
		CONICAL WALL	CYLINDRICAL WALL	TOTAL WALL			
1	0.0 - 20.0	0	0	0			
2	20.0 - 37.5	0	0	0			
3	37.5 - 72.5	0	0	0			
4	72.5 - 90.0	0	0	0			
5	90.0 - 107.5	0	0	0			
6	107.5 - 125.0	0	2.857	1.428	0.0076	172.55	152.55
7	125.0 - 142.5	0	11.428	5.715	0.0041	177.35	157.35
8	142.5 - 160.0	68.572	85.715	77.143	0.0022	180.06	160.06
9	160.0 - 177.5	31.428	0	15.714	0.0012	181.52	161.52
10	177.5 - 195.0	0	0	0			
11	195.0 – 200.0	0	0	0			
TOTAL		100	100	100			

CHAPTER VII

CONCLUSION

A two-dimensional CFD for short-form spray dryer was developed and compared with published experimental results and predictions. The comparison study shows good agreement between the model and published experiment and prediction result for gas velocity and temperature profiles.

The objective of this research is to study the effect of fluid flow pattern and key parameter to wall deposition problem within a spray dryer.

7.1 Fluid flow pattern

Three patterns of the droplet direction are observed: (1) droplets fall down and go out the dryer, (2) droplets hit the conical wall and then fall down along the wall of the chamber and (3) droplets hit and move upward to the top of the chamber at the side wall and then recirculate downward to the bottom.

7.2 Prediction wall deposition

7.2.1 Viscous stress and friction velocity

Viscous stress and friction velocity in the axial direction are key factors to explain a wall deposition problem. Droplets are possibly attached to the wall at the position that the viscous stress and friction velocity show their maximum values. The maximum friction velocity region is at the conical wall, which is the same region as the viscous stress in the axial direction. Viscous stress is dominated by the force in the axial direction. So the droplets are possibly attached at the maximum viscous stress region.

Effect of the conical wall angle on the viscous stress along the axial direction. When the height of side wall and diameter of chamber increase, they decrease the angle of the conical wall. The maximum viscous stress in the axial direction increases as the angle of the conical wall is less than its nominal value

Effect of inlet fluid velocity on the wall deposition problem is indicated that a linear relationship of the inlet velocity of feed droplets and the maximum viscous stresses, the viscous stress increases with increased inlet velocity.

7.2.2 Glass transtion temprature and sticky temperature

Stickiness of powder can be explained by a low glass transition temperature (T_g) of components with low molecular weight. Glass transition temperature (T_g) is a

reference parameter to project the spray drying systems and characterize the properties, quality, stability and safety of product. Drying agent material has reducing the stickiness and wall deposition in spray drying. Maltodextrin was able to significantly increase the T_g compared with pure water.

Higher DE value of maltodextrin led to particles with lower glass transition temperatures, it has significantly increase glass transition temperature (T_g), reduce hygroscopicity of the final product and reduce particle attach the wall. Humidity of droplet increases, as the result of the glass transition temperature of system decreases.

7.2.3 Particle impact position

Temperature range 160.0 - 177.5 °C has higher than glass transition temperature, as the results of particles are in a sticky state and attach the walls 68.571%. Particles are attached on the conical wall more than cylindrical wall.

Effect of wall heat transfer coefficient found that high of heat transfer coefficient useful to decrease the wall temperature. Heat transfer coefficient of the wall changes, the temperature of the gas at the wall as the heat transfer coefficient reduction, temperature of the gas at the wall will be higher. On the contrary, heat transfer coefficient increased, as the resulted of a decrease in the temperature of gas at the wall. The distribution of wall temperature indicates that there is low stickiness on most parts of the dryer wall.

REFERENCES

Adhikari, B., Howes, T., Shrestha, A.K., and Bhandari, B.R. (2007). Development of whey protein isolate and lactose droplets during convective drying. **Chemical Engineering and Processing** 46 : 420-428.

Bahandari, B.R., Senoussi, A., Dumoulin, E.D., and Albert, A. (1993). Spray drying of concentrated fruit juices. **Drying Technology** 11 : 1081-1092.

Bhandari, B., and Howes, T. (2005). Relating the stickiness property of foods undergoing drying and dried products to their surface energetics. **Drying Technology** 23 : 791-797.

Bhandari, B.R., Datta, N., and Howes, T. (1997a). Problems associated with spray drying of sugar-rich foods, **Drying Technology** 15 : 671.

Bhandari, B.R. (1997b). A semi-empirical approach to optimize the quantity of drying aids required to spray dry sugar-rich foods, **Drying Technology** 15 : 2509.

Bird, R.B., Stewart, W.E. and Lightfoot, E.N., **Transport Phenomena**, pp.76-200, John Wiley & Sons Inc., New York, 1960.

Boonyai, P., Bahandari, B., and Howes, T. (2004). Stickiness measurement techniques for food powders: A Review. **Powder Technology** 145 : 34-46.

Brennan, J. G., Herrera, J., and Jowitt, R. (1971). A study of some of the factors affecting the spray drying of concentrated orange juice, on a laboratory scale, J. **Food Technology** 6 : 295.

Cánovas, B.G.V., Rivas, O.E., Juliano, P., and Yan, H. Encapsulation Processes, In : Food powders: Physical Properties, Processing, and Functionality, Chapter 8, pp.199-219. 2005.

Chegini, G.R., and Ghobadian, B. Estimating the regression based mathematical models of orange juice powder physical properties with operating variable of spray dryer. **Proceedings of the IWSIS Symposium**, Mumbai, India. 2004.

Chiou, D., and Langrish, T.A.G. Crystallization of amorphous spray dried powders. In Proceedings of 15th International Drying Symposium (IDS 2006), Budapest, Hungary, 2006, pp. 562569.

Choudhury, D., Introduction to the Renormalization Group Method and Turbulence Modeling, FLUENT Inc. Technical Memorandum TM-107, 1993.

Crowe, C.T., Modeling spray air contact in spray drying systems, in Advances in drying, ed by Mujumdar, A.S., Hemi-sphere: New York, vol. 1, pp. 63-99, 1980.

Dobry, D.E., Settell, D.M., Baumann, J.M., Ray, R.J., Graham, L.J., and Beyerinck, R.A. (2009). A model-based methodology for spray-drying process development. **J. Pharm Innov**. 4 : 133-142.

Dolinsky, A., Maletskaya, Y., and Snezhkin, Y. (2000). Fruit and vegetable powders production technology on the bases of spray and convective drying methods. **Drying Technology** 18 : 747-758.

Ferziger, J.H. and Meric, M., Computational Methods for Fluid Dynamics, 2nd Ed., pp.24-237, Berlin; New York; Springer, 1999.

Fletcher, D. F., Guo, B., Harvie, D. J. E., Langrish, T. A. G., Nijdam, J. J., and Williams, J. What is important in the simulation of spray dryer performance and how do current CFD models perform. Third International Conference on CFD in the Minerals and Process Industries. Melbourne. 2003.

Fletcher, D.F., Guo, B., Harvie, D., Langrish, T.A.G., Nijdam, J.J., and Williams, J. (2006). What is important in the simulation of spray dryer performance and how do current CFD models perform?. **Applied Mathematical Modeling**, 11 : 1281-1292.

Fluent Manual, Chapter 2, materials; chapter 19: Discrete Phase Models; Chapter 20, Turbulence model, www.fluent.com, 2004.

Furuta, T., Hayashi, H. and Ohashis, T.,(1994). Some criteria of spray dryer design for food design, **Drying technology**, 12(1&2) : 151-177.

Gibson, M.M. and Launder, B.E.,(1978). Ground Effects on Pressure Fluctuations in the Atomospheric Boundary Layer, **J. Fluid Mech.**, 86 : 491-511.

Hayashi, H. (1989). Drying technologies of foods their history and future, **Drying Technology** 7 : 315369.

Hinze, J.O., **Turbulence**, pp. 16-78, McGraw-Hill Publishing Co., New York, 1975.

Huang, L., Kumar, K., and Mujumdar, A.S. (2006). A comparative study of a spray dryer with rotary disc atomizer and pressure nozzle using computational fluid dynamic simulations. **Chem. Eng. Process** 45 : 461-470.

Huntington D.H. (2004). The influence of the spray drying process on product properties, **Drying Technology** 22 : 1261–1287.

Kajiyama, T., and Park, K.J. INFLUENCE OF AIR PARAMETERS ON SPRAY DRYING ENERGY CONSUMPTION, Revista Brasileira de Produtos Agroindustriais, Campina Grande, 12 (2010) : 45-54, ISSN 1517-8595.

Keey, R.B. Introduction to Industrial Drying Operations. Pergamon, Oxford, UK, (1978) : 15–99.

Kieviet, F.G. Modelling Quality in Spray Drying, Ph.D. Thesis, T.U. Eindhoven, The Netherlands. 1997.

Kieviet, F.G.; Raaij, J.V.; Moor, P.P.E.A.D. and Kerkhof, P.J.A.M.,(1997). Measurement and Modelling of the Air Flow Pattern in a Pilot-plant Spray Dryer; **Trans. I. Chem. E.**, 75 (A) : 321-328.

Kota, K., and Langrish, T.A.G. (2006). Fluxes and patterns of wall deposits for skim milk in a pilot-scale spray dryer. **Drying Technology** 24 : 993–1001.

Kuo, K.K.Y., Principles for Combustion, pp. 10-225 John Wiely and Sons, New York, 1986.

Kurialose, R., and Anandharakrishnan, C. (2010). Computational fluid dynamics (CFD) applications in spray drying of food products, **trends in Food Science & Technology**. 21 : 383-398.

Langrish, T.A.G. (2009). Multi-scale mathematical modeling of spray dryers. **Journal of Food Engineering** 93 : 218-228.

Langrish, T.A.G., Williams, J., and Fletcher, D.F. (2004). Simulation of the effects of inlet swirl on gas flow patterns in a pilot-scale spray dryer. **Chemical Engineering Research and Design** 82 : 821-833.

Langrish, T.A.G., and Zbicinski, I. (1994). The Effects of Air Inlet Geometry and Spray Cone Angle on the Wall Deposition Rate in Spray Dryers. **Transaction of IChemE** 72 : 420-430.

Launder, B.E., (1989) Second-Moment Closure: Present… and Future? inter. **J. Heat Fluid Flow**, 10(4) : 282-300.

Launder, B.E., Reece, G.J. and Rodi, W., (1975). Progress in the Development of a Reynolds-Stress Turbulence Closure, **J. Fluid Mech.**, 68(3) : 537-566.

Launder, B.E. and Spalding, D.B., Lectures in mathematical models of turbulence, pp. 10-128, Academic press, London, England, 1972

Launder, B.E. and Spalding, D.B.,(1974). The Numerical Computation of Turbulent Flows, **Comput. Methods Appl. Mech. Eng.**, 3 : 269-289.

Lazar, W. E. et al. (1956). Experimental production of tomato powder by spray drying, **Food Technology** 3: 129.

LeBarbier, C., Kockel, T.K., Fletcher, D.F., and Langrish, T.A.G. (2001). Experimental measurement and numerical simulation of the effect of swirl on flow stability in spray dryers, **Trans IChemE**, Part A, 79: 260–268.

Lo, S. (2005). Application of computational fluid dynamics to spray drying. **Lait** 85: 353- 359.

Masters, K. Deposit-free spray drying: dream or reality? In Proceedings of the 10th International Drying Symposium (IDS '96), Drying '96, Krakow, Poland, C. Strumillo and A.S. Mujumdar, Eds. Lodz Technical University, Lodz, Poland, Vol. A, 52, 1996.

Masters, K. Spray drying. An introduction to principles, operational practice and applications. Leonard Hill Books; London, 1972.

Moller, T.J., and Fredsted S. Cover Story: A primer on spray drying. Chemical engineering. www.CHE.com. pp. 40 november 2009.

Mujumdar, A.S., Dryers for particulate solids, slurries and sheet-form materials, in Mujumdar's Practical Guide to Industrial Drying, ed by Devahastion, S., pp. 37-71, Exergex corporation, Montreal, 2000

Mujumdar, A.S. Handbook of industrial drying 2nd Edn., Marcel Dekker, New York, pp: 1238. 1987.

Oliveira, W.P., Souza, C.R.F., Kurozawa, L.E., and Park, K.L. Spray drying of food and herbal products - Volume 1, Ed. Woo, M.W., Mujumdar, A.S. and Daud, W.R.W. ISBN - 978-981-08-6270-1, Published in Singapore, pp. 113-156. 2010.

Ozmen, L., and Langrish, T.A.G. (2003). An Experimental Investigation of the Wall Deposition of Milk Powder in a Pilot-Scale Spray Dryer. **Drying Technology** 21 : 1253-1272.

Palzer, S. (2005). The effect of glass transition on the desired and undesired agglomeration of amorphous food powders, **Chem. Eng. Sci.** 60 : 3959–3968.

Ranz, W.E. and Marshall, W.R.,(1952a). Evaporation from drops, **Chem. Eng. Prog.**, 48: 141-146.

Ranz, W.E. and Marshall, W.R.,(1952b). Evaporation from drops, **Chem. Eng. Prog.**, 48 : 173-180.

Roos, Y.H., and Karel M. (1991). Water and molecular weight effects on glass transition in amorphous carbohydrates and carbohydrate solutions, **J. Food Sci.** 56 : 1676–1681.

Shih, T., Liou, W., Shabbir, A. and Zhu, J.,(1995). A New $\sum\Box k$ Eddy-Viscosity Model for High Reynolds Number Turbulent Flows-Model Development and Validation, **Computers Fluids**, 24(3) : 227-238.

Southwell, D.B., and Langrish, T.A.G. (2001). The effect of swirl on flow stability in spray dryers. **Trans. I. Chem. E.** 79 : 222–234.

Straatsma, J., Van Houwelingen, G., Steenbergen, A.E., and De Jong, P. (1999). Spray Drying of Food Products: Simulation Model. **Journal of Food Engineering** 42 : 67-72.

Strumillo, C., and Kudra, T. Drying: Principles, Application and Design. Gordon and Breach, New York, NY, (1986) : 45–54.

Truong, V., Bhandari, B.R., and Howes, T. (2005). Optimization of co-current spray drying process of sugar-rich foods. Part I Moisture and glass transition temperature profile during drying. **Journal of Food Engineering**, 71 : 55.

Ullum, T. Simulation of a spray dryer with rotary atomizer: The appearance of vortex breakdown. Proceedings of the 15th International Drying Symposium (2006) : 251-257.

Verdumen, R.E.M., Menn, P., Ritzert, J., Blei, S., Nhumaio, G.C.S., Sorenson, T.S., Gunsing, M., Straatsma, J., Verschueren, M., Sibeijn, M., Schulte, G., Fritsching, U., Bauckhage, K., Tropea, C., Sommerfeld, M., Watkins, A.P., Yule, A.J., Schonfeldt, H. (2004). Simulation of Agglomeration in Spray Drying Installations: The EDECAD Project. **Drying Technology** 22 : 1403-146.

Wang, W., and Zhou, W. (2013). Water Adsorption and Glass Transition of Spray-Dried Soy Sauce Powders Using Maltodextrins as Carrier, *Food and Bioprocess Technology*, 6(10), 2791-2799.

Welti, J.S., and Lafuenete, B. (1983). Spray drying of comminuted orange products. **Chemical Engineering Progress**, 79: 80-85.

Werner, S.R.L., Jones, J.R., and Paterson, A.H.J., (2007). Stickiness of maltodextrins using probe tack test during in-situ drying, **J. Food Eng**. 80: 859–868.

Woo, M.W., Daud, W.R.W., Mujumdar, A.S., Wu, Z.H., Talib, M.Z.M., and Tasirin, S.M. (2009). Steady and transient flow simulations in short-form spray dryers. **Chemical Product and Process Modeling** 4.

VITA

Artitaya Patniboon was born in Khonkaen, Thailand. After graduating high school from Nomphongsuksa School in Namphong, she entered the King Mongkut's Institute of Technology Ladkrabang, Ladkrabang, Bangkok and received the degree of Bachelor of Engineering (Food Engineering) in March 31, 2011. In June, 2011, she began to study his Master degree in Chemical Engineering at Chulalongkorn University and joined the Control and Systems Engineering Research Center.